Journal of Inorganic Biochemistry 257 (2024) 112600

Contents lists available at ScienceDirect

Journal of Inorganic Biochemistry

journal homepage: www.elsevier.com/locate/jinorgbio

The impact of biomolecule interactions on the cytotoxic effects of rhenium (I) tricarbonyl complexes

Tayná Saraiva de Lavor [a,1], Maria Henriqueta Silvestre Teixeira [b,1], Patrícia Alves de Matos [a], Ricardo Campos Lino [b], Clara Maria Faria Silva [b], Marcos Eduardo Gomes do Carmo [c], Marcelo Emílio Beletti [d], Antonio Otavio T. Patrocinio [c], Robson José de Oliveira Júnior [b,*], Tayana Mazin Tsubone [a,*]

[a] Laboratório Interdisciplinar de Fototerapia e Biomoléculas (LIFeBio), Instituto de Química (IQ), Universidade Federal de Uberlândia (UFU), Uberlândia, Minas Gerais, Brazil
[b] Laboratório de Citogenética, Instituto de Biotecnologia (IBTEC), Universidade Federal de Uberlândia (UFU), Uberlândia, Minas Gerais, Brazil
[c] Laboratory of Photochemistry and Materials Science, Chemistry Institute, Federal University of Uberlândia, Uberlândia, Minas Gerais, Brazil
[d] Instituto de Ciências Biomédicas (ICBIM), Universidade Federal de Uberlândia (UFU), Uberlândia, Minas Gerais, Brazil

ARTICLE INFO

Keywords:
Anti-cancer drugs
Rhenium complexes
Biomolecules
Cytotoxicity
Drug design
Organometallic complexes

ABSTRACT

Rhenium complexes show great promise as anticancer drug candidates. Specifically, compounds with a Re$(CO)_3(NN)(py)^+$ core in their architecture have shown cytotoxicity equal to or greater than that of well-established anticancer drugs based on platinum or organic molecules. This study aimed to evaluate how the strength of the interaction between rhenium(I) tricarbonyl complexes *fac*-[Re$(CO)_3$(NN)(py)]$^+$, NN = 1,10-phenanthroline (phen), dipyrido[3,2-f:2′,3′-h]quinoxaline (dpq) or dipyrido[3,2-a:2′3’-c]phenazine (dppz) and biomolecules (protein, lipid and DNA) impacted the corresponding cytotoxic effect in cells. Results showed that *fac*-[Re$(CO)_3$(dppz)(py)]$^+$ has higher Log $P_{o/w}$ and binding constant (K_b) with biomolecules (protein, lipid and DNA) compared to complexes of *fac*-[Re$(CO)_3$(phen)(py)]$^+$ and *fac*-[Re$(CO)_3$(dpq)(py)]$^+$. As consequence, *fac*-[Re$(CO)_3$(dppz)(py)]$^+$ exhibited the highest cytotoxicity (IC_{50} = 8.5 μM for HeLa cells) for *fac*-[Re$(CO)_3$(dppz)(py)]$^+$ among the studied compounds (IC_{50} > 15 μM). This highest cytotoxicity of *fac*-[Re$(CO)_3$(dppz)(py)]$^+$ are probably related to its lipophilicity, higher permeation of the lipid bilayers of cells, and a more potent interaction of the dppz ligand with biomolecules (protein and DNA). Our findings open novel avenues for rational drug design and highlight the importance of considering the chemical structures of rhenium complexes that strongly interact with biomolecules (proteins, lipids, and DNA).

1. Introduction

The search for new anticancer drugs is still ongoing, as well-established drugs containing platinum, such as cisplatin, carboplatin, and oxaliplatin, have demonstrated resistance and severe side effects during treatment [1]. Thus, the primary challenge for scientists in advancing anticancer research is to achieve minimal or negligible side effects for novel therapeutic avenues in the field. In recent decades, several metal complexes have shown great potential as anticancer drug candidates [1]. The main reason for this is the flexibility of metal complexes in adopting various types of chemical structures that enable them to engage in effective binding interactions with target biomolecules, thereby enhancing their effectiveness [2].

Among transition metal complexes, rhenium (Re) organometallic complexes demonstrate noteworthy characteristics, such as facile synthesis *via* a one-step strategy, remarkable thermal and kinetic stability, and excellent photochemical and photophysical properties [2]. Anticancer applications of rhenium complexes have only recently been

Abbreviations: Re$(CO)_3$, rhenium(I) tricarbonyl complexes; py, pyridine; phen, 1,10-phenantroline; dpq, dipyrido[3,2-f:2′,3′-h]quinoxaline; dppz, dipyrido[3,2-a:2′3’-c]phenazine; IR, infrared; RMN, ^{1}H Nuclear Magnetic Resonance; BSA, bovine serum albumin; DNA, deoxyribonucleic acid; DOPG, 1,2-dioleoyl-sn-glycero-3-phospho-(1′-rac-glycerol) (sodium salt)..

* Corresponding authors.
E-mail addresses: oliveirajunior@ufu.br (R.J. de Oliveira Júnior), tayana.tsubone@ufu.br (T.M. Tsubone).

[1] These authors contributed equally to the work.

https://doi.org/10.1016/j.jinorgbio.2024.112600
Received 1 March 2024; Received in revised form 26 April 2024; Accepted 7 May 2024
Available online 10 May 2024

explored [3]. In particular, compounds comprising a $Re(CO)_3$ core in their architecture have shown the possibility of overcoming the limitations of platinum-based drugs [4]. Several studies have demonstrated the therapeutic potential of these compounds [5–9]. Knopf et al. have conducted research on various rhenium tricarbonyl complexes to evaluate their anticancer properties [6]. They discovered a drug candidate that demonstrates greater potency than cisplatin against HeLa cells [6]. This particular complex trigger cell death through a unique mechanism, different from that of cisplatin, thereby avoiding cross-resistance between the two compounds [6]. Further studies on *in vivo* biodistribution and metabolites of the complex have verified its stability and indicated its excretion through the renal and hepatobiliary systems [6].

Leonidova and colleagues have discussed the cytotoxic Re organometallic complexes mainly focused on IC_{50} values and their modes of cytotoxic action [1]. Most of the reported cytotoxic effects toward human cancer cell lines present remarkable outcomes associated with rhenium complexes characterized by the general formula *fac*-$Re(CO)_3$, exhibiting IC_{50} values <30 μM [1]. The toxicity of the compounds typically rose with their lipophilicity, likely because of enhanced uptake by cells [1]. Enslin et al. demonstrated remarkably low cytotoxicity (IC_{50} = 30–50 nM) of Re(I) carbonyl complexes against prostate adenocarcinoma (PC3) [10]. The exceptional toxicity was attributed to the compounds' localization in mitochondria and nuclei, leading to the downregulation of mitochondrial ATP production in PC3 cells [10]. Although recent studies have shown the potential of Re tricarbonyl complexes as anticancer drugs [1,5–10], there remains a gap in the understanding of the influence of biomolecule interactions with rhenium(I) tricarbonyl complexes on their cytotoxic effects in cells.

Recently, Konkankit and colleagues showed that one of the factors contributing to the increased cytotoxic activity of rhenium(I) tricarbonyl complexes was their lipophilic and hydrophilic nature [11]. They demonstrated that by increasing the alkyl chain length of $Re(CO)_3$, cellular uptake was swifter, and cytotoxic effects manifested on a significantly accelerated timescale [11]. Although this study elucidates the influence of the lipophilic/hydrophilic nature of rhenium(I) tricarbonyl complexes in modulating the rate of cell death, it is not clear how lipophilic characteristics can influence the combination of Re complex with biomolecules (*i.e.*, proteins, lipids, and DNA) for optimizing its intrinsic pharmacological properties. Expanding on previous efforts, the objective of this study was to examine how the interactions of the Re complex with biomolecules affect cell death. In this context, we aimed to prepare a series of $Re(CO)_3$ molecules with different ligand characteristics (Fig. 1) to understand the relationship between lipophilicity, strength of biomolecule binding, and cytotoxicity.

2. Experimental section

2.1. Synthesis and characterization of rhenium(I) tricarbonyl complexes

$ReCl(CO)_5$, 1,10-phenantroline (phen), pyridine (py), and trifluoromethanesulfonic acid were purchased from Aldrich (Darmstadt, Germany) and used without further purification. The ligands, dipyrido[3,2-f:2′,3′-h]quinoxaline (dpq) and dipyrido[3,2-a:2′3′-c]phenazine (dppz) were synthesized as described previously [12–14]. The *fac*-[$Re(CO)_3(NN)(py)]PF_6$ complexes, NN = phen (1), dpq (2), and dppz (3), were prepared according to previously described procedures [15–18]. Product purity was confirmed by elemental analysis, infrared (IR) and ^{1}H Nuclear Magnetic Resonance (NMR).

Attenuated total reflectance Fourier-transformed infrared (ATR-FTIR) spectra were recorded in a Perkin Elmer Frontier spectrometer equipped with a diamond crystal plate, using 16 scans at a resolution of 2 cm^{-1}. ^{1}H NMR spectra were recorded in a Bruker Ascend 400 MHz spectrometer using the residual solvent signal as internal standard. Elemental analysis was carried out in a Perkin Elmer 2400 CHNS analyzer. Electronic absorption spectra were recorded in a Shimadzu UV–Vis spectrophotometer UV-1650 PC. Room temperature emission measurements were performed in argon degassed CH_3CN solutions in a 1.000 cm quartz cuvette. Emission quantum yields were determined taking the *fac*-[$ClRe(CO)_3$(phen)] as standard (φ_{em} = 0.018 in CH_3CN at 298 K) [19].

fac-$[Re(CO)_3(phen)(py)]^+$: IR (cm^{-1}): $\nu_{C\text{-}H(arom)}$ w(3088), $\nu_{C\text{-}H(arom)}$ w(2970), $\nu_{C\equiv O}$ s(2013), $\nu_{C\equiv O}$ s(1922), $\nu_{C\equiv O}$ s(1872), $\nu_{C=C(arom)}$ m(1627), $\nu_{C=C(arom)}$ m(1601), $\nu_{C=N(arom)}$ m(1583), $\nu_{C=N(arom)}$ m(1518), $\nu_{C=N(arom)}$ m(1490), $\nu_{P\text{-}F}$ s(850), $\nu_{C\text{-}H(arom)}$ s(722), $\nu_{C\text{-}H(arom)}$ m(641), $\nu_{P\text{-}F}$ s(546), $\nu_{Re\text{-}N}$ s(271).

fac-$[Re(CO)_3(dpq)(py)]^+$: IR (cm^{-1}): $\nu_{C\text{-}H(arom)}$ w(3093), $\nu_{C\text{-}H(arom)}$ w(3044), $\nu_{C\equiv O}$ s(2019), $\nu_{C\equiv O}$ s(1916), $\nu_{C\equiv O}$ s(1870), $\nu_{C=C(arom)}$ m(1608), $\nu_{C=C(arom)}$ m(1577), $\nu_{C=N(arom)}$ w(1547), $\nu_{C=N(arom)}$ m(1530), $\nu_{C=N(arom)}$ m(1479), $\nu_{P\text{-}F}$ m(824), $\nu_{C\text{-}H(arom)}$ m(730), $\nu_{C\text{-}H(arom)}$ m(644), $\nu_{P\text{-}F}$ m(526), $\nu_{Re\text{-}N}$ m(277).

fac-$[Re(CO)_3(dppz)(py)]^+$: IR (cm^{-1}): $\nu_{C\text{-}H(arom)}$ w(3088), $\nu_{C\text{-}H(arom)}$ w(2923), $\nu_{C\equiv O}$ s(2032), $\nu_{C\equiv O}$ s(1936), $\nu_{C\equiv O}$ s(1908), $\nu_{C=C(arom)}$ w(1605), $\nu_{C=C(arom)}$ w(1578), $\nu_{C=N(arom)}$ w(1547), $\nu_{C=N(arom)}$ m(1495), $\nu_{C=N(arom)}$ w(1465), $\nu_{P\text{-}F}$ s(834), $\nu_{C\text{-}H(arom)}$ s(807), $\nu_{C\text{-}H(arom)}$ m(637), $\nu_{P\text{-}F}$ m(530), $\nu_{Re\text{-}N}$ w(271).

For *fac*-$[Re(CO)_3(phen)(py)]PF_6$ (1), the yield was 87%, and anal. Calcd. for $ReC_{20}H_{13}N_3O_3PF_6$: C, 35.61%; N, 6.23%; H, 1.94%, found: C, 35.14%; N, 6.06%; H, 2.16%. ^{1}H NMR (400 MHz, CD_3CN) d 10.36 (dd, 2H, *J* 1.32, 5.10 Hz), 9.59 (dd, 2H, *J* 1.36, 8.10 Hz), 9.02 (dd, 2H, *J* 1.48, 6.50 Hz), 8.92 (s, 2H), 8.87 (dd, 2H, *J* 5.12, 8.11 Hz), 8.50 (m, 1H), 7.94 (m, 2H).

For *fac*-$[Re(CO)_3(dpq)(py)]PF_6$ (2), the yield was 92%. calcd. For $ReC_{25}H_{22}N_5O_3PF_6$: C, 47.91%; N, 11.18%; H, 3.54%, found: C, 47.86%; N, 11.05%; H, 3.36%. ^{1}H NMR (400 MHz, CD_3CN) d 10.54 (dd, 2H, *J*

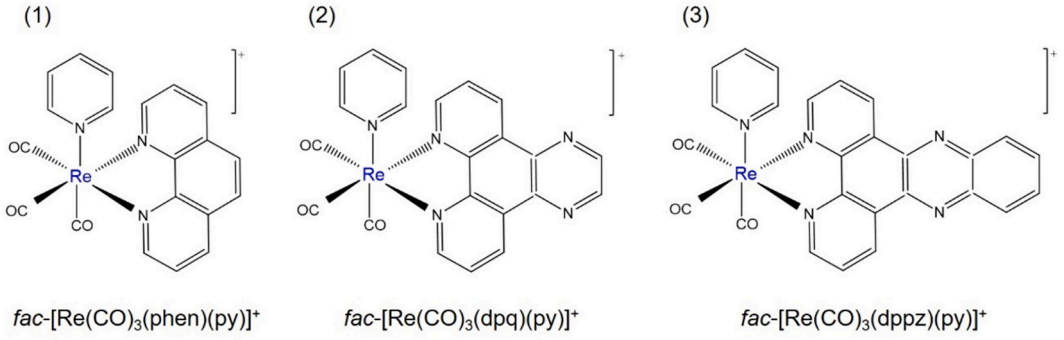

Fig. 1. Rhenium(I) tricarbonyl complexes examined in this study are listed as follows: (1) *fac*-$[Re(CO)_3(phen)(py)]^+$; (2) *fac*-$[Re(CO)_3(dpq)(py)]^+$ and (3) *fac*-$[Re(CO)_3(dppz)(py)]^+$.

1.24, 8.40 Hz), 10.44 (dd, 2H, *J* 1.48, 5.14 Hz), 9.95 (s, 2H), 9.06 (dd, 2H, *J* 1.40, 6.38 Hz), 9.01 (dd, 2H, *J* 5.40, 8.46 Hz), 8.50 (m, 1H), 7.96 (m, 2H).

For *fac*-[Re(CO)$_3$(dppz)(py)]PF$_6$ (3), the anal yield was 79%. calcd. For $ReC_{26}H_{15}N_5O_3PF_6$: C, 40.01%; N, 8.97%; H, 1.94%; found: C, 39.86%; N, 8.75%; H, 1.80%. ^{1}H NMR (400 MHz, CD_3CN) d 10.66 (dd, 2H, *J* 1.36, 8.30 Hz), 10.42 (dd, 2H, *J* 1.32, 5.28 Hz), 9.22 (dd, 2H, *J* 3.36, 6.52 Hz), 9.11 (dd, 2H, *J* 1.52, 6.64 Hz), 9.02 (dd, 2H, *J* 5.28, 8.30 Hz), 8.89 (dd, 2H, *J* 3.20, 6.68 Hz), 8.52 (m, 1H), 7.99 (m, 2H).

2.2. Partition coefficient determination of rhenium(I) tricarbonyl complexes

The coefficient of partitioning of the rhenium complexes was determined using octanol and water in a shake-flask method according to the method described in previous studies [20,21]. Briefly, the rhenium complex (50 μM) was added to a mixture consisting of octanol and water in a 50% (*v*/v) ratio. After intense stirring, the samples were incubated in the dark for 24 h. The organic phase was then separated from the aqueous phase, and the Re(I) complex concentration in each phase was evaluated using UV–vis spectroscopy. The coefficient of partitioning in the octanol phase (log $P_{o/w}$) was determined using Eq. (1) [22]:

$$\boldsymbol{Log\ P_{o/w} = Log_{10}\left(\frac{[ReComplex]_{octanol}}{[ReComplex]_{water}}\right)} \quad (1)$$

where $[ReComplex]_{octanol}$ and $[ReComplex]_{water}$ represent the molar concentrations of the Re(I) complex in octanol and water.

The experiment was performed in independent duplicates, with three repetitions in each experiment ($n = 6$), and the average and standard deviation of the log $P_{o/w}$ values obtained in each experiment were calculated.

2.3. Bovine serum albumin (BSA)-binding assay by fluorescence analysis

Interactions between rhenium(I) complexes and bovine serum albumin (BSA) were studied using spectroscopic techniques. The solution of BSA (3 μM) was prepared in Tris buffer (10 mM, pH 7.4). Then, fluorescence spectra of BSA (3 μM, in Tris buffer 10 mM, pH 7.4) were recorded in the absence or presence of the rhenium(I) tricarbonyl complexes (with concentrations ranging from 0 to 16 μM in Tris buffer with <1.0% *v*/v DMSO) ($\lambda_{ex} = 280$ nm, slit widths of 5.0 nm for excitation and 1.0 nm for emission) in the range 300–450 nm at 35 °C.

Because each rhenium complex exhibited notable absorption at the excitation and emission wavelengths (280 and 350 nm, respectively), the inner filter effect was adjusted using Eq. (2) [23]:

$$\mathbf{F_{cor} = F_{obs}\ 10^{[(A_{ex}+A_{em})/2]}} \quad (2)$$

F_{cor} and F_{obs} denote the corrected and observed fluorescence intensity values, respectively, whereas A_{ex} and A_{em} represent the experimental absorbance values at the excitation and emission wavelengths, respectively.

The quenching constants were calculated from Stern-Volmer Eq. (3):

$$\frac{F_0}{F} = 1 + k_q.\tau_0\ [Q] = 1 + K_{SV}.[Q] \quad (3)$$

where F_0 and F are the fluorescence intensities in the absence and presence of the quencher, respectively, K_{SV} is the Stern–Volmer quenching constant, k_q is the bimolecular quenching constant, τ_0 is the average lifetime of the Trp-214 residue without the quencher (~1×10^{-8} s) [23] and [Q] is the concentration of the quencher.

The modified Stern–Volmer equation was employed to calculate the binding constant (K_b) and number of binding sites (*n*) (Eq. (4)) [24]:

$$\boldsymbol{log\frac{(F_0 - F)}{F} = logK_b + nlog[Q]} \quad (4)$$

where F_0 and F are the fluorescence intensities in the absence and presence of the rhenium complex, respectively, and [Q] is the quencher (in this case, the rhenium complex).

2.4. Liposome-binding assay by UV–Vis spectroscopy

For liposome preparation, lipid films of DOPG were produced by evaporating chloroform in argon air, followed by hydration with 2.0 mL of Tris buffer (10 mM, pH 7.4) solution [25,26]. Stock DOPG lipid concentration was 1.5 mM. All vesicle suspensions were extruded 21 times through polycarbonate membranes comprising pores with a diameter of 100 nm using an Avanti Mini-Extruder [27].

Solutions of each rhenium complex (20 μM in Tris buffer with <1.0% *v*/v DMSO) were prepared. The changes in Re(I) complex (20 μM) absorption spectra were followed with successive small-volume additions of DOPG liposomes (1.5 μM). The incubation time needed to achieve equilibrium was 30 min (data not shown), as determined experimentally. Then, after each addition of an aliquot of DOPG liposomes (1.5 μM) and incubation of 30 min, the absorption spectra of Re(I) complex (20 μM) were recorded in the range 210–800 nm at room temperature.

The binding constant (K_b) of the rhenium complex to liposomes was calculated using Eq. (5), as previously described [28,29]:

$$\mathbf{A} = \frac{\mathbf{A_0 + A_f K_b[L]}}{\mathbf{1 + k_b[L]}} \quad (5)$$

where A is the rhenium complex absorbance intensity recorded in the presence of the lipid at concentration [L], A_0 is the rhenium complex absorbance measured in the absence of the lipid, and A_f is the asymptotic value of the absorbance of the complete rhenium complex.

2.5. DNA-binding assay by UV–Vis spectroscopy

A straightforward method for assessing the potential interactions between DNA and a drug involves monitoring alterations in the absorption properties of either the drug or DNA molecules [30].

A solution of salmon sperm DNA (*ss*-DNA) was prepared by dissolving 5 mg of *ss*-DNA in 5 mL of Tris buffer (50 mM) containing NaCl (5 mM) at pH 7.4 [31]. The DNA solution with a ratio of absorbance of approximately 1.8 recorded at 260 and 280 nm (Abs_{260nm}/Abs_{280nm}) indicates that the DNA was sufficiently free of protein and that the double helix structure was intact [32,33]. Thus, before starting the experiment, DNA integrity was checked by ensuring that $Abs_{260nm}/Abs_{280nm} \geq 1.8$, and *ss*-DNA concentration was calculated using the molar absorption coefficient, $\varepsilon_{260} = 6600\ M^{-1}\ cm^{-1}$ [32,33]. The stock *ss*-DNA solution was refrigerated at 2–10 °C using an ice bath during all experiments.

Solutions of each Re(I) complex were adjusted to a fixed concentration of 20 μM in Tris buffer (50 mM) and NaCl (5 mM) containing <1.0% *v*/v acetonitrile at a pH of 7.4. Then, after each addition of 10 μL of aliquots of *ss*-DNA solution, the mixture containing the Re(I) complex was incubated with DNA for 5 min, and the absorption spectrum with varying *ss*-DNA concentrations (0–50 μM) was recorded in the range 210–800 nm at room temperature.

The binding constant (K_b) was obtained from the intercept-to-slope ratios of $A_0/(A - A_0)$ *vs.* 1/[DNA] according to the following Eq. (6) [30,34]:

$$\frac{A_0}{A - A_0} = \frac{\varepsilon_G}{\varepsilon_{HG} - \varepsilon_G} * \frac{1}{K_b[DNA]} \quad (6)$$

where A_0 is the absorbance of the complex in the absence of DNA, A is the absorbance in the presence of DNA at concentration [DNA], and ε_G and ε_{HG} are the absorption coefficients of the rhenium complex and the

[ReComplex]–DNA, respectively.

2.6. Molecular docking and ligand preparation

The ligands were designed using the Avogadro software version 1.1.1 and saved in mol^2 format after structural optimization. The files were then configured in Avogadro software using the extensions tool to obtain an optimized geometry in a Universal Force Field (UFF). In AutoDock 1.5.7, the ligands were prepared by adding polar hydrogen atoms and Gasteiger charges, and possible water molecules were deleted.

Molecular docking studies of the metallocomplexes of rhenium were carried out using the Auto Dock 1.5.7 software with DNA and BSA biomolecules. The crystal structures of DNA (126D) with a sequence of CATGGCCATG at a resolution of 2 Å and BSA (3 V03) at a resolution of 2.7 Å were obtained from the Protein Data Bank (www.rcsb.org). Polar hydrogen atoms and Kollman charges were added to the structure, and the water molecules around the DNA/BSA were removed.

To study the binding state in blind docking, the DNA was analyzed in a grid box with dimensions of 62 × 58 × 96 for the three complexes. BSA was analyzed by considering the location of two possible binding sites in the region of tryptophan 134 with the coordinates x = 45.989286, y = 36.667143, and z = 25.500143, and tryptophan 213 with the coordinates x = 101.169786, y = 28.225500, and z = 19.778429.

For the BSA binding study, two possible sites were analyzed in a 70x76x78 scan box. Lamarkian genetic algorithms were used to perform the ligand-receptor binding calculations. The number of genetic algorithm runs was set to 100, and the number of evaluations was set to 2.5 million [35,36] The DNA/BSA interactions were produced using Biovia Discovery Studio Visualizer version 2021 and Maestro Schrödinger software, version 13.6.122.

2.7. DNA cleavage studies

To investigate the interaction of the complexes with DNA, we combined the *fac*-$[Re(CO)_3(phen)(py)]^+$, *fac*-$[Re(CO)_3(dpq)(py)]^+$, and *fac*-$[Re(CO)_3(dppz)(py)]^+$ complexes with plasmid DNA from the siSTRIKE™ U6 Hairpin Cloning System (Human) – hMGFP. The isolated plasmid was incorporated into a series of 11 solutions, each with a total volume of 20 μL. These solutions included 30 ng/μL of the plasmid treated at the concentrations of 40 μM and 80 μM of *fac*-$[Re(CO)_3(phen)(py)]^+$ and *fac*-$[Re(CO)_3(dpq)(py)]^+$ and 10 μM and 20 μM of *fac*-$[Re(CO)_3(dppz)(py)]^+$ in PBS 1× with or without dimethyl sulfoxide (DMSO - 0.05%), hydrogen peroxide (H_2O_2–15 mM), and a combination of both. Controls consisted of an untreated plasmid, a plasmid treated with the unique site restriction enzyme *Xba* I, and a plasmid treated with H_2O_2. The reaction mixtures underwent incubation at 37 °C for 12 h, followed by the addition of 3 μL of loading buffer (loader - 0.25% bromophenol blue, 0.25% xylene cyanol, 30% glycerol, 10 mM EDTA). Subsequently, electrophoresis was conducted on a 0.8% agarose gel containing 0.05% ethidium bromide (10 μg/mL) in 90 mM Tris-borate buffer (pH 8.0) and 20 mM EDTA (0.5 × TBE). Gel electrophoresis was performed at 80 V for 3 h, and the results were examined under ultraviolet light. Bands were quantified using the ImageJ software version 1.53 k (Java 1.8.0_172).

2.8. Cytotoxicity of rhenium(I) tricarbonyl complexes

The HeLa cell line, derived from cervical cancer cells, was obtained from the American Type Culture Collection (ATCC) and cultivated in Dulbecco's Modified Eagle's Medium (DMEM) supplemented with 10% fetal bovine serum (FBS), 100 μg/ml penicillin, and 100 μg/mL streptomycin. PNT2 (human prostate epithelial cell line), B16-F10 (murine melanoma cells), and NIH/3 T3 (murine fibroblasts) were cultured in RPMI-1640 medium (Gibco®, Paisley, UK) supplemented with 2 mM/L glutamine, 25 mM HEPES, 100 μg/mL penicillin, 100 μg/mL streptomycin, and 10% fetal bovine serum (FBS). All cultures were maintained in a 5% CO_2 atmosphere at 37 °C.

A cell viability assay using the MTT method was used to assess the cytotoxicity of Re (I) complexes [37,38]. Cells were grown to 70–80% confluence in a 75 cm^2 flask, detached with trypsin/EDTA, seeded in 48-well plates at a density of 3×10^4 cells/well in 300 μL of the growth media, and incubated at 37 °C in an atmosphere containing 5% CO_2 for 24 h. Compounds were dissolved in DMSO to prepare stock solutions and subsequently diluted in growth media (DMEM, 10% FBS, 100 μg/ml penicillin, and 100 μg/ml streptomycin) to maintain a DMSO concentration of <1%. Following removal of the medium, cells were incubated with fresh medium (300 μL) containing varying concentrations (0–100 μM) of the desired rhenium complex for 24 h at 37 °C in an atmosphere containing 5% CO_2. The growth medium containing the Re(I) complex was removed and incubated for an additional 24 h to allow adequate time for cell proliferation. Subsequently, 100 μL of MTT (0.75 mg/mL) was added to 300 μL of DMEM comprising 10% FBS. After 3 h, the MTT/DMEM solution was removed, and formazan crystals were dissolved in 300 μL of DMSO. The absorbance of each well was measured at 570 nm using a microplate reader. Cell viability was calculated by normalizing the absorbance of the treated cells to that of the untreated cells (without the complex; normalized to 100% cell viability). The percentage cell viability and IC_{50} values shown in this study represent the average of two independent experiments with three replicates per concentration level. For IC_{50} analysis (concentration that inhibits 50% of cell growth), GraphPad Prism 8.0 software (GraphPad Software Inc., La Jolla, California, USA) was used based on nonlinear regression, where the percentage of cell viability was determined as a base 10 logarithmic function of the concentrations tested assuming a 95% confidence interval ($p < 0.05$).

To assess the selectivity of the complexes against tumor cells, the selectivity index (SI) was calculated as the ratio between the concentrations needed to reduce cell viability by 50% (IC_{50}) in non-tumor cells and tumor cells. The following formula was used: SI = (IC_{50} of the non-tumor lineage)/(IC_{50} of the tumor lineage). An SI ≥ 2 designated the compound as more selective for tumor cell lines, indicating it kills twice as many neoplastic cells as healthy cells. This designation underscores its potential as a promising anticancer candidate [39].

2.9. Cell cycle analysis by flow cytometry

To explore the potential antiproliferative effects of the rhenium metallocomplexes, HeLa tumor cells (2×10^5 cells/mL) were incubated with varying concentrations of different complexes. In this study, *fac*-$[Re(CO)_3(phen)(py)]^+$ and *fac*-$[Re(CO)_3(dpq)(py)]^+$ were administered at concentrations of 10 μM, 20 μM, and 40 μM, whereas *fac*-$[Re(CO)_3(dppz)(py)]^+$ was employed at concentrations of 5 μM, 10 μM, and 20 μM, with the selected concentrations aligning with their respective IC_{50} values. The cells were incubated for 24 h. Subsequently, the cells were centrifuged for 10 min at 1000 rpm, resulting in a pellet that underwent two washes with PBS1× and subsequent fixation in a 70% ethanol solution in PBS 1×. The fixed samples were stored at 4 °C overnight. Subsequently, the cells were centrifuged for 10 min at 1000 rpm, and the pellet was re-suspended in PBS 1× containing 10 μg/ml propidium iodide and 100 μg/ml RNase. This step aims to eliminate RNA contamination, allowing only DNA to be stained. The cells were then incubated in the dark for 45 min at 37 °C, after which the samples were subjected to analysis using the ACCURI flow cytometer (BD). The analysis was conducted on the FL2 channel, and the obtained cytometric data were analyzed using the FloJo software (version 10).

2.10. Statistical analysis

Octave 7.2.0 was utilized for comparative statistical analyses. The data, which were derived from a minimum of two (often three) independent experiments, were presented as mean values ± standard error (SE). Initially, adherence to a Gaussian curve was assessed for pairwise

comparisons. Subsequently, depending on the nature of the data, parametric or non-parametric analyses were performed using Student's *t*-test or Holm-Sidak test for independent samples. Multiple comparisons were performed using one-way analysis of variance (ANOVA) with Tukey or Bonferroni tests, based on variance homogeneity and the number of groups involved. The strength of the linear correlation was determined using Pearson's coefficient (r). Statistical significance was set at a threshold of $P < 0.05$. In the figures, significance levels concerning the control are denoted with asterisks above the bars, and multiple or pairwise comparisons are indicated accordingly.

3. Results and discussion

3.1. Synthesis and photophysical properties

The photophysics of the *fac*-[Re(CO)$_3$(NN)(py)]$^+$ employed in this study have been extensively discussed in a previous study [15]. As shown in Fig. 2, the electronic absorption and emission spectra of the complexes in acetonitrile were obtained at 298 K. The main absorption and physical parameters are summarized in Table 1.

The parent complex *fac*-[Re(CO)$_3$(phen)(py)]$^+$ exhibited high-energy fully allowed absorption bands attributed to the internal IL ($\pi \rightarrow \pi^*$) transitions in the phen ligand. Low-energy metal-to-ligand charge transfer (MLCT) absorption was observed at 370 nm (Fig. 2), which was responsible for the main photophysical properties of the fluid solution at room temperature. A typical broad emission band was observed following light excitation (Fig. 2), which was attributed to ^{3}MLCT radiative decay, as discussed elsewhere [15].

The replacement of the phen ligand by dpq and then dppz led to redshifts in the high-energy absorption bands, owing to the extended conjugation of the quinoxaline and phenazine ligands (Fig. 2). In *fac*-[Re(CO)$_3$(dpq)(py)]$^+$, the MLCT transition was associated with the lowest energy absorption band, whereas in *fac*-[Re(CO)$_3$(dppz)(py)]$^+$, an overlap of the MLCT and IL transitions was observed, leading to an increase in the molar absorptivity coefficient (ε) (Table 1). The stabilization of the IL excited states in *fac*-[Re(CO)$_3$(dpq)(py)]$^+$ and *fac*-[Re(CO)$_3$(dppz)(py)]$^+$ also led to considerable changes in the emission properties. The complex with dpq maintained its ^{3}MLCT emitter state with an emission maximum demonstrating a red-shift by ~12 nm compared to *fac*-[Re(CO)$_3$(phen)(py)]$^+$, albeit with a smaller quantum yield and emission lifetime (Table 1). In contrast, for *fac*-[Re(CO)$_3$(dppz)(py)]$^+$, a structured emission band was observed, which was attributed to radiative decay of the triplet intraligand excited state (^{3}IL$_{dppz}$). As expected, the quantum yield was one order of magnitude smaller, and the corresponding lifetime reached 108 μs (Table 1).

Table 1
Photophysical data for the studied complexes in acetonitrile at 298 K (λ_{exc} = 375 nm) [15].

Rhenium(I) Complex	λ_{max} (nm) (ε / 10^4 (L mol^{-1} cm^{-1}))	λ_{em} (nm)	ϕ_{em}	τ / μs
fac-[Re(CO)$_3$(phen)(py)]$^+$	222 (4.11), 252 (2.71), 275 (3.40), 327 (0.72), 369 (0.48)	545	0.020	1.6
fac-[Re(CO)$_3$(dpq)(py)]$^+$	258 (5.43), 286 (2.73), 370 (0.50)	557	0.012	0.45
fac-[Re(CO)$_3$(dppz)(py)]$^+$	278 (8.98), 362 (1.85), 381 (1.81)	554, 600	0.001	108

3.2. Partition coefficient of rhenium(I) tricarbonyl complexes

Drug absorption in an organism is mediated *via* passage through biological membranes. The lipophilicity of drug molecules strongly influences receptor binding, cellular uptake, and bioavailability [40]. During this process, hydrophilic or hydrophobic pathways are employed to transport the substance to its site of action, where it can exert its biological effects. The octanol-water partition coefficient (log $P_{o/w}$) is useful for estimating the simple relationship between hydrophilic/hydrophobic characteristics and biological responses, such as IC_{50} values [41]. Thus, the octanol/water partition coefficient (log $P_{o/w}$) was assessed to evaluate the lipophilic and hydrophilic nature of the rhenium(I) complexes (Table 2).

While positive log $P_{o/w}$ values indicate a greater affinity of the compound for the organic phase, negative log $P_{o/w}$ values indicate an affinity for the aqueous phase [42]. The log $P_{o/w}$ value obtained for *fac*-[Re(CO)$_3$(dppz)(py)]$^+$ was positive and larger than that of the other investigated complexes (Table 2). This indicates that *fac*-[Re(CO)$_3$(dppz)(py)]$^+$ exhibited greater affinity for the organic phase, probably because it is the most lipophilic molecule among the rhenium

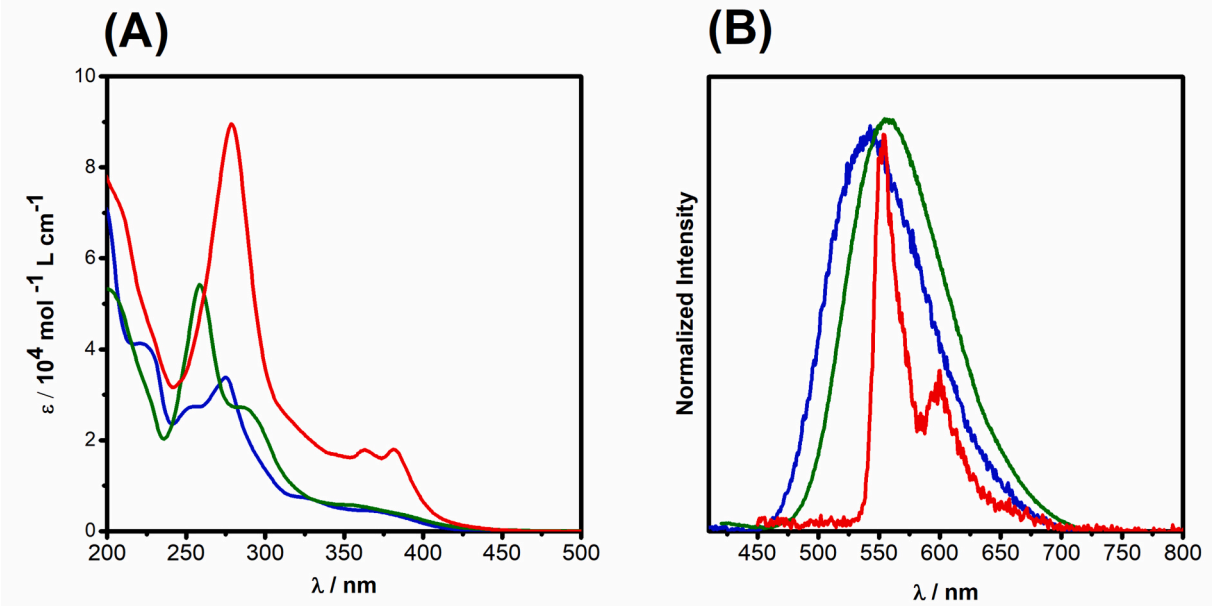

Fig. 2. Absorption (A) and emission (B) spectra of studied complexes in acetonitrile at 298 K. [Re(CO)$_3$(phen)(py)]$^+$ (blue), [Re(CO)$_3$(dpq)(py)]$^+$ (green), and [Re(CO)$_3$(dppz)(py)]$^+$ (red). λ_{exc} = 375 nm. (For interpretation of the references to colour in this figure legend, the reader is referred to the web version of this article.)

Table 2
Log $P_{o/w}$ of the studied rhenium(I) tricarbonyl complexes. The values correspond to the mean ± standard deviation (SD) from two separate assays with three replications in each experiment ($n = 6$).

Rhenium(I) complex	Log $P_{o/w}$
fac-[Re(CO)$_3$(phen)(py)]$^+$	−0.39 ± 0.08
fac-[Re(CO)$_3$(dpq)(py)]$^+$	−0.15 ± 0.11
fac-[Re(CO)$_3$(dppz)(py)]$^+$	+0.65 ± 0.21

complexes studied. The two negative Log $P_{o/w}$ values for the complexes of *fac*-[Re(CO)$_3$(phen)(py)]$^+$ (Log $P_{o/w} = -0.39 \pm 0.08$) and *fac*-[Re(CO)$_3$(dpq)(py)]$^+$ (Log $P_{o/w} = -0.15 \pm 0.11$) corresponded to greater affinity for the aqueous phase (Table 2). These Log $P_{o/w}$ values are comparable to other reports, which show a Log $P_{o/w}$ of −0.11 for a less hydrophobic rhenium complex (*fac*-[Re(phen)(CO)$_3$(PyCH$_2$O-daminozide)]PF$_6$) and Log $P_{o/w}$ of +0.65 for a more hydrophobic molecule (*fac*-[Re(DIP)(CO)$_3$(PyCH$_2$O-daminozide)]PF$_6$) [4].

The observed log $P_{o/w}$ values exhibited an ascending order: *fac*-[Re(CO)$_3$(phen)(py)]$^+$ < *fac*-[Re(CO)$_3$(dpq)(py)]$^+$ < *fac*-[Re(CO)$_3$(dppz)(py)]$^+$ (Table 2), reflecting the hydrophobic characteristics of their ligands (Fig. 1). Hence, the more hydrophobic the NN ligand of the rhenium complex, the higher the log $P_{o/w}$ value. This finding is in line with other reports showing that incorporating longer alkyl chains into the ligands of rhenium(I) tricarbonyl complexes also increases the log $P_{o/w}$ values [11].

3.3. Binding constant (K_b) for the interaction of rhenium(I) complex with BSA

Serum albumin is a primary protein in the mammalian circulatory system. This macromolecule plays an important physiological role in blood pH control and improves the solubility of hydrophobic molecules in aqueous media [43]. Therefore, it is crucial to study the interactions between the drug candidates and these proteins. BSA has frequently been employed as a protein model in these studies [43,44]. Despite their importance, only a few studies have investigated the interactions between rhenium complexes and BSA [43–45]. Therefore, the ability of the rhenium(I) tricarbonyl complexes to interact with BSA was investigated.

Typically, steady-state fluorescence techniques allow for the straightforward determination of protein-molecule binding parameters. Albumins exhibit fluorescence emission due to the aromatic amino acid residues present in the protein (*e.g.*, tryptophan and tyrosine). When a small molecule binds to albumin, the protein microenvironment is altered, and the fluorescence intensity of the protein is affected [23]. Therefore, the interaction between BSA and *fac*-[Re(CO)$_3$(NN)(py)]$^+$ was determined by the fluorescence quenching of the protein. The successive addition of rhenium complexes to BSA led to a reduction in the fluorescence intensity of the protein (Fig. 3A and Fig. S1 in the supplemental material). Stern–Volmer quenching constants and binding parameters were determined (Table 3) as described in the experimental section using Eq. (3) for fitting plots of log[(F_0/F)/F] *versus* log [ReComplex] (Fig. 3B and Fig. S2 in the supplemental material).

From the fluorescence quenching results it is possible to obtain parameters such as Stern-Volmer constant (Ksv) and the quenching rate constants (k_q) (Table 3). The rhenium complexes showed high values of the quenching constant (Ksv > 10^4 M^{-1}) indicating their great efficiency to interact strongly with BSA. k_q values were much greater than the maximum quenching rate constant of diffusion collision of 2.0×10^{10} M^{-1} s^{-1} (Table 3), suggesting that complex formation between BSA and rhenium complexes may involve both types of quenching mechanisms, dynamic and static [23]. To unravel whether the interaction mechanism is static or dynamic, time-resolved fluorescence studies should be performed. However, investigation about the type of suppression mechanism is not the goal of this work. We are focused to estimate the strength of interaction between [ReComplex]-BSA (*via* K_b), instead of the mechanism of BSA interaction.

The number of binding sites (n) indicated that the rhenium(I) tricarbonyl complexes bound to BSA in a 1:1 ratio (Table 3), which is in agreement with other reports [44,45]. The [ReComplex]-BSA K_b values increased in the following order: *fac*-[Re(CO)$_3$(phen)(py)]$^+$ < *fac*-[Re(CO)$_3$(dpq)(py)]$^+$ < *fac*-[Re(CO)$_3$(dppz)(py)]$^+$ (Table 3). These data corroborated the results obtained for log $P_{o/w}$ values, which followed the same trend (Table 2). This indicates that greater hydrophobicity of the rhenium complex favors a stronger interaction with the protein.

3.4. Binding constant (K_b) for the interaction of rhenium(I) complex with liposome

Liposomes, which are lipid bilayer vesicles frequently employed as models for cell membranes in permeability and diffusion studies, can be tailored to mimic various membrane structures by adjusting the lipid

Table 3
Stern–Volmer constants (Ksv), the quenching rate constants (k_q), binding constant (K_b) and number of binding sites (n) in rhenium(I) tricarbonyl complexes for BSA.

Rhenium (I) complex	Ksv (×10^4 M^{-1})	K_b (×10^3 M^{-1})	k_q (M^{-1} s^{-1})	n	R^2
fac-[Re(CO)$_3$(phen)(py)]$^+$	4.26 ± 0.10	3.10 ± 0.07	4.26 × 10^{12}	0.91	0.968
fac-[Re(CO)$_3$(dpq)(py)]$^+$	2.19 ± 0.17	8.57 ± 0.26	2.19 × 10^{12}	0.99	0.873
fac-[Re(CO)$_3$(dppz)(py)]$^+$	13.7 ± 0.78	25.7 ± 0.24	1.38 × 10^{13}	0.99	0.984

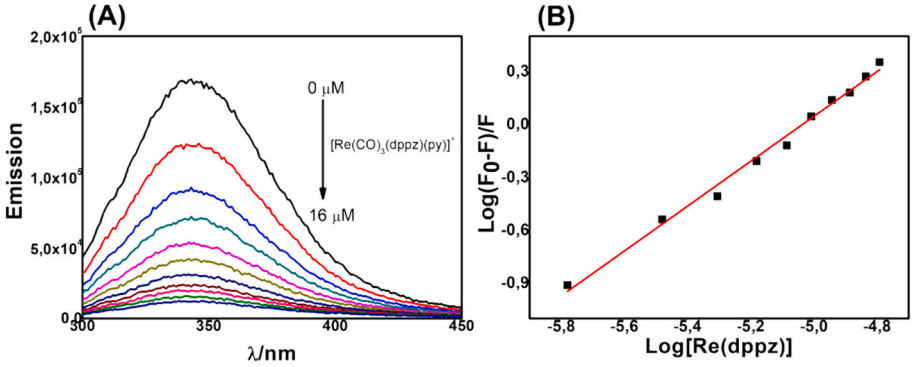

Fig. 3. (A) Emission spectra of BSA (3.0 μM in Tris buffer, pH 7.4) with successive additions of [Re(CO)$_3$(dppz)(py)]$^+$ (ranging from 0 to 16 μM in Tris buffer with <1.0% *v*/v DMSO). Temperature: 35 °C. λ_{exc} = 280 nm with excitation and emission slits of 5.0 nm and 1.0 nm, respectively. **(B)** The plot depicting log[(F_0/F)/F] *versus* log[[Re(CO)$_3$(dppz)(py)]$^+$] in presence of BSA.

composition [46]. The behavior of rhenium complexes in the presence of cell membranes and their lipophilic characteristics can be assayed by their interactions with liposomes [46]. The strength of the interaction between the rhenium complexes and liposomes was assessed using UV–Vis spectroscopy. The methodology comprises altering the intensity of absorption after the incorporation of liposomes into molecules and considers that a chemical equilibrium occurs between the binding molecule and the lipid bilayer to obtain a conventional binding isotherm [29]. Aliquots of liposomes (DOPG) were added to a solution of the rhenium complexes (Fig. 4A and Fig. S3 in the supplemental material). Binding constant values (K_b) shown in Table 4 were calculated by adjusting a theoretical model (Eq. (4), described in the experimental section) derived from the experimental points on the plot of absorbance at λ_{max} calculated as a function of DOPG concentration (Fig. 4B and Fig. S4 in the supplemental material).

The absorbance intensity of the three rhenium complexes increased, even at a fixed concentration (20 μM), when aliquots of liposomes (DOPG) were added (Fig. 4A and Fiugre S3 in the supplemental material). The observed [ReComplex]-liposomes K_b values exhibited an ascending order: *fac*-$[Re(CO)_3(phen)(py)]^+$ < *fac*-$[Re(CO)_3(dpq)(py)]^+$ < *fac*-$[Re(CO)_3(dppz)(py)]^+$ (Table 4). The ascending order of these K_b values aligns with the data for log $P_{o/w}$ (Table 2) and K_b values for proteins (Table 3), suggesting that the hydrophobic nature of *fac*-$[Re(CO)_3(dppz)(py)]^+$ favors the interaction of the rhenium complex with biomolecules.

Table 4
Binding constant (K_b) for the interaction between rhenium(I) tricarbonyl complexes and DOPG liposomes. Values represent the average ± standard deviation of two independent experiments.

Rhenium(I) complex	K_b ($\times 10^3$ M^{-1})
fac-$[Re(CO)_3(phen)(py)]^+$	2.14 ± 0.08
fac-$[Re(CO)_3(dpq)(py)]^+$	4.71 ± 0.10
fac-$[Re(CO)_3(dppz)(py)]^+$	15.29 ± 1.74

3.5. Binding constant (K_b) for the interaction of rhenium (I) complex with DNA

Many drugs currently in clinical use or in advanced clinical trials pharmacologically target DNA. Certain molecules can bind to DNA, thereby inhibiting cell replication, which is a critical process in cell growth and division [47]. Metal-based anticancer complexes primarily target DNA by binding to the N-7 position of guanine residues [30]. Studying the interactions of drug candidates with DNA is important for the rational design of new drugs. UV–Vis spectroscopy is employed to study drug-DNA interactions, given that the intercalative binding of a complex with DNA can result in a hypochromic and/or bathochromic shift in the absorption spectrum [30]. To substantiate the potential binding of each rhenium complex to DNA, the binding constant (K_b) was computed by tracking changes in absorbance as the concentration of DNA increased (Fig. S5 in the supplemental material). The DNA biomolecule exhibited an absorption band (260 nm) in the same region as the IL bands of the Re complexes (250–300 nm); Fig. S6. To enable data analysis in the 250–300 nm region, the UV–Vis absorption spectrum of DNA alone (without Re complexes) was recorded under the same conditions used in the assay in the presence of complexes (Fig. S7 in the supplemental material). Thus, the absorbance spectra of the compounds in the presence of various concentrations of DNA (Fig. S5) were subtracted from the absorbance of the DNA spectra alone in the absence of Re molecules (Fig. S7) to evaluate the spectral changes in the region of 250–300 nm. A representative spectrum of *fac*-$[Re(CO)_3(dppz)(py)]^+$ after successive additions of DNA is shown in Fig. 5A (see data from other rhenium complexes in Fig. S8 in the supplemental material). The value of K_b was obtained as the ratio of the slope to the intercept obtained from the plot of $A_0/A\text{-}A_0$ *versus* 1/[DNA] (Fig. 5B and Fig. S9 in the supplemental material) and is summarized in Table 5Table.

The absorption spectrum of the Re complexes without interference from the characteristics of DNA absorption (Fig. 5A and Fig. S8) showed alterations in the absorbance intensity in the region spanning from 250 to 300 nm attributed to an increase in the concentration of DNA, which was verified for all studies performed in triplicate. A hypochromic effect (reduced absorbance) was observed with the *fac*-$[Re(CO)_3(phen)(py)]^+$ and *fac*-$[Re(CO)_3(dppz)(py)]^+$ complexes (Fig. S8A and Fig. 5A), suggesting intercalating-type interactions due to π-π-type stacking between ligands in the complex with the nitrogenous bases of DNA [30]. In contrast, the complex *fac*-$[Re(CO)_3(dpq)(py)]^+$ showed a hyperchromic effect (Fig. S8B), in contrast with previous studies. The observed hyperchromism suggests that *fac*-$[Re(CO)_3(dpq)(py)]^+$-DNA interactions primarily involve electrostatic interactions or interactions with the DNA groove attributed to the destabilization of the double helix [48]. To conclusively support that *fac*-$[Re(CO)_3(phen)(py)]^+$ and *fac*-$[Re(CO)_3(dppz)(py)]^+$ complexes display an intercalative DNA binding interaction and *fac*-$[Re(CO)_3(dpq)(py)]^+$ primarily involve interactions that destabilize the DNA double helix, additional experiments still would be needed, such as viscosity, thermal denaturation and/or circular dichroism [8,49–53]. Nevertheless, our research primarily focused to assess the strength of the interaction between [ReComplex]-DNA (*via* K_b) rather than the mechanism of DNA interaction.

The strength of [ReComplex]-DNA interaction (K_b) exhibited the following ascending order: *fac*-$[Re(CO)_3(phen)(py)]^+$ < *fac*-$[Re(CO)_3(dpq)(py)]^+$ < *fac*-$[Re(CO)_3(dppz)(py)]^+$ (Table 5). The K_b values were comparable to those of other metal complexes that bind to DNA reported in literature [8,30,54,55]. Again, *fac*-$[Re(CO)_3(dppz)(py)]^+$ showed the highest K_b value with DNA, corroborating previous data showing the highest K_b value with BSA and the highest log $P_{o/w}$ among the studied compounds. This emphasizes the importance of the

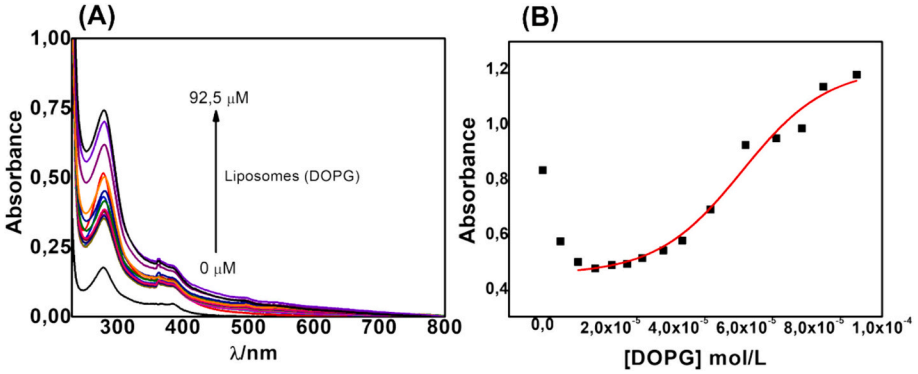

Fig. 4. (A) Absorption spectra of *fac*-$[Re(CO)_3(dppz)(py)]^+$ (20 μM) with successive addition of DOPG liposomes (1.5 μM) in Tris buffer, pH 7.4 at room temperature. (B) Plot of *fac*-$[Re(CO)_3(dppz)(py)]^+$ absorbance at $\lambda_{maximum}$ *versus* [DOPG] used for the calculation of K_b values.

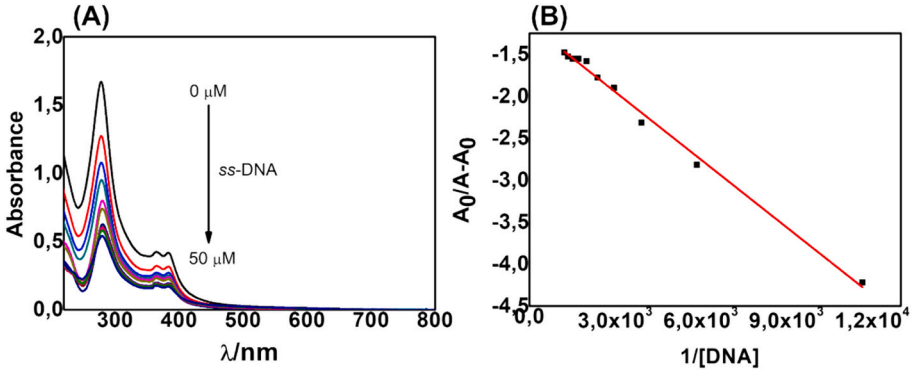

Fig. 5. **(A)** Absorption spectra of *fac*-[Re(CO)$_3$(dppz)(py)]$^+$ (20 μM) discounting the absorption spectra of *ss*-DNA at different concentrations in Tris buffer (50 mM) and NaCl (5 mM) at pH 7.4 and room temperature. **(B)** Plot of $A_0/A\text{-}A_0$ *versus* 1/[DNA] obtained to calculate K_b value of *fac*-[Re(CO)$_3$(dppz)(py)]$^+$.

Table 5
Binding constant (K_b) of the interaction between rhenium(I) tricarbonyl complexes and DNA. Values represent the mean ± standard error of three independent experiments ($n = 3$).

Rhenium(I) complex	K_b ($\times 10^3$ M^{-1})
fac-[Re(CO)$_3$(phen)(py)]$^+$	1.35 ± 0.52
fac-[Re(CO)$_3$(dpq)(py)]$^+$	2.01 ± 0.77
fac-[Re(CO)$_3$(dppz)(py)]$^+$	7.63 ± 0.44

hydrophobicity of the dppz ligand, which favors enhanced interaction with the hydrophobic regions of biomolecules (proteins, lipids, and DNA).

3.6. Molecular docking

As *in vitro* analyses revealed that the complexes can interact with important cellular biomolecules, *in silico* simulations were performed using bioinformatics tools. This study aimed to enhance our understanding of the potential chemical bonds that could form between Re complexes and BSA proteins or DNA.

3.7. In silico molecular interactions of fac-[Re(CO)$_3$(phen)(py)]$^+$, fac-[Re(CO)$_3$(dpq)(py)]$^+$, and fac-[Re(CO)$_3$(dppz)(py)]$^+$ with BSA

Molecular docking revealed interactions between the three Re complexes and BSA macromolecules at the examined activation sites exhibiting low binding energies indicative of favorable binding. The data in Table 6 demonstrate an inverse relationship between the hydrophobicity of the Re complexes and the binding energy, indicating a more favorable binding affinity with an increase in the the hydrophobicity. This is consistent with the experimental findings for K_b with BSA, supporting the observation that a more hydrophobic Re complex corresponds to a higher K_b (Table 3).

Fig. 6A, C, and E depict the interactions of *fac*-[Re(CO)$_3$(NN)(py)]$^+$ complexes with BSA in chain A near the tryptophan 134 site. Conversely, Fig. 6B, D, and F illustrate their interactions in chain B, which is close to the tryptophan 213 site.

Table 6
The energy of the interactions between rhenium complexes and the BSA molecule at tryptophan sites 134 (chain A) and 213 (chain B).

Rhenium(I) complex	Binding energy Tryptophan 134 (kcal/mol)	Binding energy Tryptophan 213 (kcal/mol)
fac-[Re(CO)$_3$(phen)(py)]$^+$	−6,72	−6,70
fac-[Re(CO)$_3$(dpq)(py)]$^+$	−7,13	−6,51
fac-[Re(CO)$_3$(dppz)(py)]$^+$	−8,97	−8,70

As depicted in Fig. 6A, interactions were observed between the pyridyl group of *fac*-[Re(CO)$_3$(phen)(py)]$^+$ and proline 117, which were mediated *via* π-alkyl hydrophobic bonds in chain A of BSA. Furthermore, the phenanthroline ligand of *fac*-[Re(CO)$_3$(phen)(py)]$^+$ engaged in π-alkyl hydrophobic interactions with isoleucine 141, leucine 115, arginine 185, and tyrosine 137 (Fig. 6A). Moving to the B chain of BSA near the tryptophan 213 site, the pyridyl group of *fac*-[Re(CO)$_3$(phen)(py)]$^+$ interacted with leucine 326, whereas phenanthroline ligand demonstrated π-alkyl hydrophobic interactions with leucine 346 and 480, valine 481 and alanine 212 (Fig. 6B). Moreover, one of the carbonyl ligands of *fac*-[Re(CO)$_3$(phen)(py)]$^+$ formed hydrogen bonds with arginine 208 (Fig. 6B).

In chain A of BSA with *fac*-[Re(CO)$_3$(dpq)(py)]$^+$ (Fig. 6C), the pyridyl group established connections with interleukin 181, tyrosine 137, and arginine 185. Simultaneously, the dipyrido[3,2-f:2′,3′-h]quinoxaline (dpq) ligand interacted with proline 117, leucine 115, lysine 114, and arginine 185. Additionally, a hydrogen bond with the nitrogen of leucine 115 was identified (Fig. 6C). Shifting to the B chain of BSA, interactions between the pyridyl ring and aspartate 450 involving anion-π interactions, as well as those with tryptophan 213 involving hydrophobic π-alkyl interactions (Fig. 6D) are depicted. In contrast, the dpq ligand of *fac*-[Re(CO)$_3$(dpq)(py)]$^+$ engaged with arginine 217 *via* cation-π interactions, lysine 221 *via* cation-π interactions, and glutamine 291 *via* hydrophobic π-alkyl interactions (Fig. 6D). Hydrogen bonds were detected between the dpq group and alanine at positions 290, 294, and 342 (Fig. 6D).

In *fac*-[Re(CO)$_3$(dppz)(py)]$^+$, the pyridyl ring interacted with interleukin 181 and tyrosine 160 (Fig. 6E). Additionally, the dipyrido[3,2-a:2′3’-c]phenazine (dppz) group of *fac*-[Re(CO)$_3$(dppz)(py)]$^+$ formed connections with tryptophan 134, leucine 115 and 122, tyrosine 137, interleukin 141, lysine 136, and proline 117 in the A chain of BSA (Fig. 6E). Furthermore, hydrogen bonds were observed between the two of their C═O groups and arginine 185 (Fig. 6E). In the B chain of BSA (Fig. 6F), hydrophobic π-alkyl interactions between the pyridyl group and valine 481, alanine 209, and 212, were detected. In contrast, the dppz ligand extended toward arginine 208 and 212 *via* hydrophobic π-cation, π-sigma interactions, and π-alkyl interactions (Fig. 6F). Hydrophobic π-alkyl interactions were also observed with alanine 209, glycine 327, alanine 349, leucine 346, lysine 350, and valine 481. Additionally, hydrogen bonds were observed between the C═O groups, leucine 480, and serine 479 (Fig. 6F).

Molecular docking analysis is a valuable tool for examining interactions between metal complexes and biological molecules, such as BSA, which plays an essential role in the transportation of ligands in the body [56].

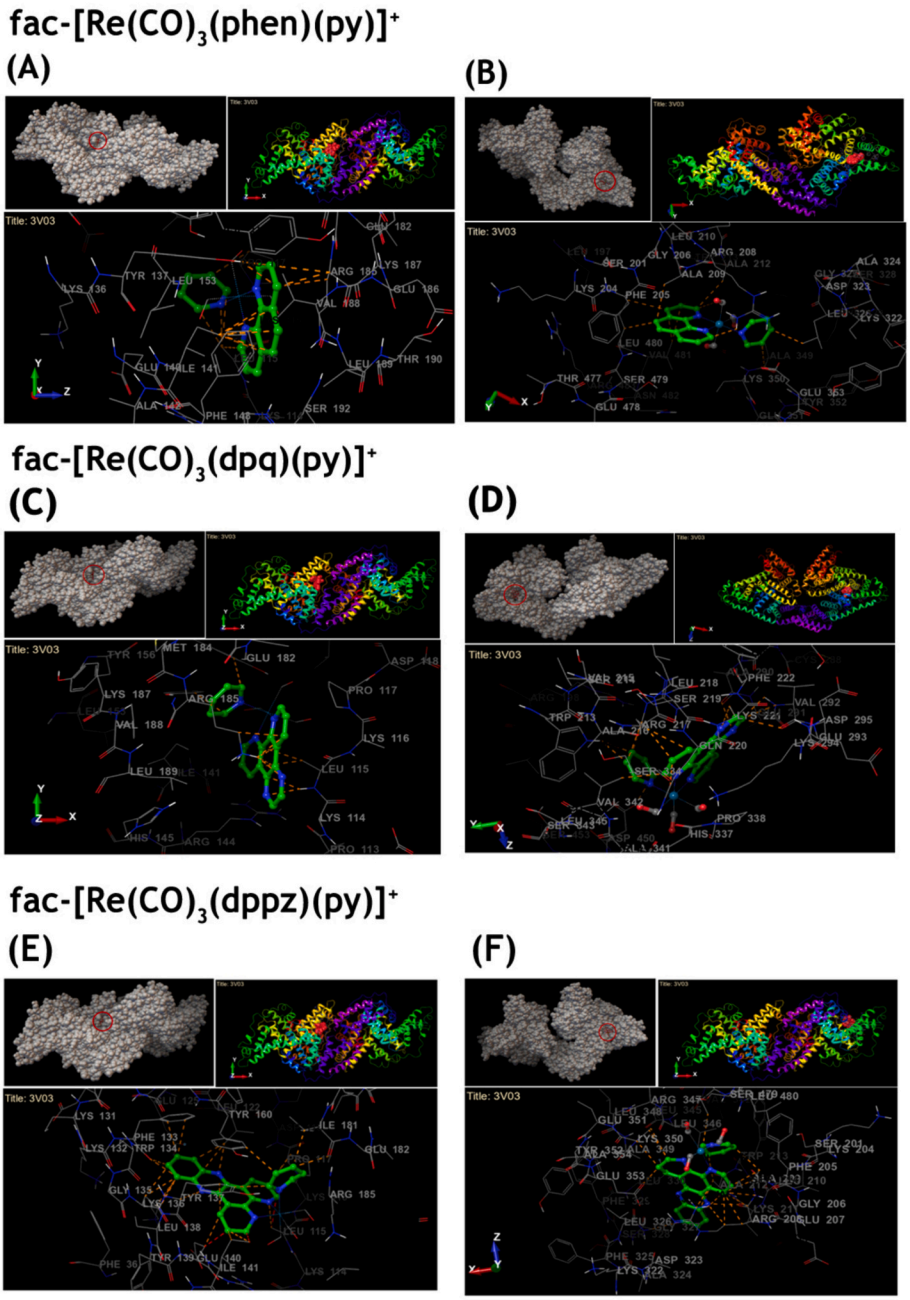

Fig. 6. Interaction between rhenium complexes with BSA protein (3 V03). **(A)** and **(B)** Interaction of *fac*-$[Re(CO)_3(phen)(py)]^+$ with the site near tryptophan 134 and tryptophan 213. **(C)** and **(D)** Interaction of *fac*-$[Re(CO)_3(dpq)(py)]^+$ with the site near tryptophan 134 and tryptophan 213. **(E)** and **(F)** Interaction of *fac*-$[Re(CO)_3(dppz)(py)]^+$ with the site near tryptophan 134 and tryptophan 213.

Our findings align with those of a previous study [44]. In their *in silico* analysis, they investigated the interaction between four rhenium complexes, specifically of the *fac*-$[Re(CO)_3(\alpha\text{-diimine})\{4\text{-C11py}\}]CF_3SO_3$ type, with BSA. Their results revealed the presence of binding sites within the hydrophobic cavities in subdomains IIA and IIIA, corresponding to sites I and II, respectively [44]. Furthermore, the identification of two amino acid residues, Trp-134 and Trp213, within BSA, both situated in subdomain IIA, demonstrated their involvement in the interaction between the complex and the protein [44]. Our research corroborates these findings, providing additional evidence for the observed interactions between the Re complex and protein.

It is important to note the existence of a hydrophobic cavity of considerable size in subdomain IIA, which can bind to various drugs. Interestingly, the Re complexes investigated in this study demonstrated the ability to bind to the same amino acid residues in subdomain IIA.

3.8. *In silico molecular interactions of fac-$[Re(CO)_3(phen)(py)]^+$, fac-$[Re(CO)_3(dpq)(py)]^+$ and fac-$[Re(CO)_3(dppz)(py)]^+$ with DNA*

Molecular docking revealed that all three complexes interacted with the DNA macromolecule, displaying low binding energies indicative of favorable binding. As shown in Table 7, an increase in the hydrophobicity of the Re complexes correlated with a decrease in the binding energy, signifying a more favorable binding affinity. This corresponds to our previously experimental results of K_b corresponding to interaction with DNA, reinforcing the observation that a Re complex with increased hydrophobicity correlates with a higher K_b value (Table 5).

The three Re complexes studied showed an affinity for the minor

Table 7
Energy associated with the interactions between rhenium complexes and the DNA molecule and number of hydrogen bonds involved in mediating the interactions.

Rhenium(I) complex	Binding energy (Kcal/mol)	Hydrogen bonds
fac-[Re(CO)$_3$(phen)(py)]$^+$	−6,78	2
fac-[Re(CO)$_3$(dpq)(py)]$^+$	−6,97	1
fac-[Re(CO)$_3$(dppz)(py)]$^+$	−7,83	1

groove in their most stable conformation. The *fac*-[Re(CO)$_3$(phen)(py)]$^+$ complex engaged with double-stranded DNA *via* adenine 8 from chain A and guanine 14 from chain B, forming hydrogen bonds (represented as green spheres in Fig. 7A).

The *fac*-[Re(CO)$_3$(dpq)(py)]$^+$ complex interacted with a single strand of DNA by forming hydrogen bonds with adenine 8 from chain A, as shown by the green spheres in Fig. 7B. In addition, *fac*-[Re(CO)$_3$(dpq)(py)]$^+$ demonstrated the ability to interact with DNA through intercalation in a less stable position.

Similarly, the *fac*-[Re(CO)$_3$(dppz)(py)]$^+$ complex exclusively

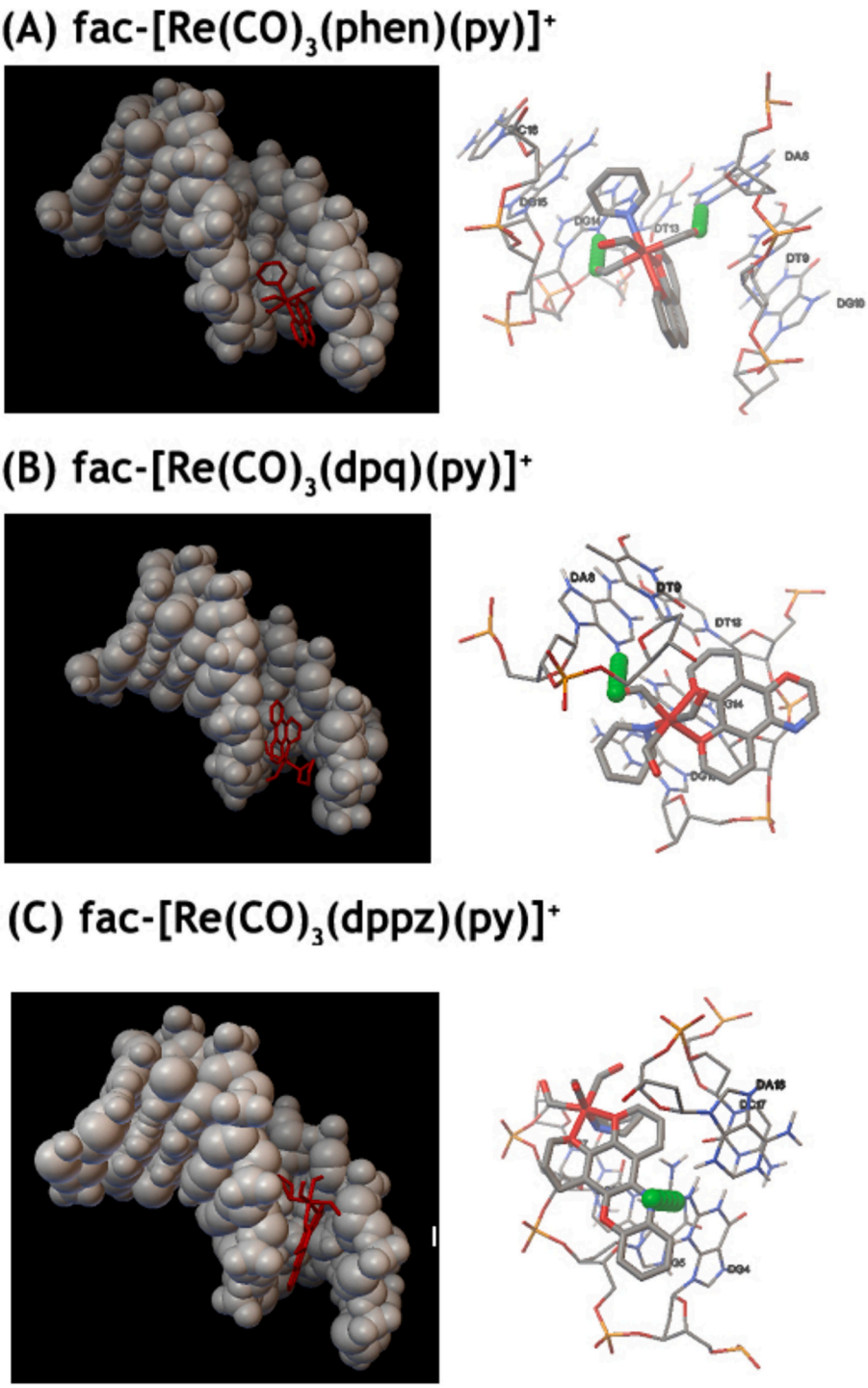

Fig. 7. Interaction between **(A)** *fac*-[Re(CO)$_3$(phen)(py)]$^+$, **(B)** *fac*-[Re(CO)$_3$(dpq)(py)]$^+$, and **(C)** *fac*-[Re(CO)$_3$(dppz)(py)]$^+$ and DNA and corresponding magnification results.

engaged with a single strand of DNA, establishing hydrogen bonds with guanine 4 from chain A, as depicted by the green spheres in the magnification shown in Fig. 7C. Similar to the previous complexes, it also exhibited other intermolecular interactions, such as van der Waals forces and induced dipole interactions.

Varma et al. synthesized rhenium complexes with heterocyclic molecular ligands and heteronuclear rhenium(I) complexes [57,58]. The interactions of these complexes with DNA were investigated *via* various spectroanalytical and electrophoretic techniques [57,58]. The results suggested that all the examined complexes bonded with the grooves of DNA and induced strand breaks [57,58]. This corroborates the molecular docking data of the three rhenium complexes reported in this study, indicating their affinity for the minor groove of DNA. Ghosh et al. noted in their molecular docking studies that rhenium(II) dinitrosyl and mononitrosyl complexes can bind to DNA, displaying a preference for orientation toward the minor groove of this biomolecule [59].

3.9. DNA cleavage studies

The interaction between rhenium complexes and DNA is crucial for identifying target structures of antitumor agents that rely on DNA cleavage. Despite the strength of binding in cases involving motifs such as dppz, DNA cleavage abilities are also influenced by other substituents present in the complexes [54]. As both UV–Vis spectroscopy results and *in silico* analyses confirmed the DNA interaction capacity, we investigated the potential of these metal complexes to induce DNA breaks using plasmids as a model.

3.10. Interaction between *fac*-[Re(CO)$_3$(phen)(py)]$^+$, *fac*-[Re(CO)$_3$(dpq)(py)]$^+$, and *fac*-[Re(CO)$_3$(dppz)(py)]$^+$ and plasmid DNA

The complex *fac*-[Re(CO)$_3$(phen)(py)]$^+$ was capable of inducing structural alterations in plasmids at different concentrations (Fig. 8A). When subjected to agarose gel electrophoresis, the untreated plasmid DNA (column 2 in the gel) predominantly exhibited a supercoiled intact form (Form I, 83.07%) and circular form with single-strand breaks (Form II, 16.93%), whereas a linear form resulting from double-strand breaks was absent (Form III). Upon treatment with [Re(CO)$_3$(phen)(py)]$^+$, the band pattern on the gel was altered, indicating the induction of both single- and double-strand breaks (columns 3 and 4 in the gel). When treated with a concentration of 80 μM (column 3 in the gel) under non-oxidative conditions, an increase in the percentage of single-strand breaks (Form II with 83.47%), a decrease in the percentage of intact supercoiled form (Form I with 5.68%), and the appearance of double-strand breaks (Form III with 10.86%) were observed.

When plasmids maintained under non-oxidative conditions were treated with DMSO, a scavenger or neutralizer of ROS (columns 5 and 6 in the gel), a decrease in the percentage of DNA in Form II (60.12%) and an increase in Form I (23.24%) were observed. Under pro-oxidative conditions represented by the introduction of hydrogen peroxide into the system, extensive plasmid degradation was observed, resulting in a smeared DNA pattern under all conditions, rendering observation of specific bands (columns 8, 9, 10, and 11) impossible.

The *fac*-[Re(CO)$_3$(dpq)(py)]$^+$ complex also induced structural alterations in the plasmids (Fig. 8B). Untreated plasmid DNA (column 2), when subjected to agarose gel electrophoresis, primarily depicted intact supercoiled form (form I at 84.69%), circular form with single-strand breaks (form II at 12.27%), and a linear form resulting from double-strand breaks with a small percentage (form III). When treated with *fac*-[Re(CO)$_3$(dpq)(py)]$^+$, the band profile of the gel was altered, indicating the induction of single-strand breaks (columns 3, 4, 5, and 6 on the gel).

In samples treated under non-oxidizing conditions, an increase in the percentage of single-strand breaks (form II) and a sharp decrease in the percentage of the intact supercoiled form (form I) were observed. Under pro-oxidizing conditions, represented by the introduction of hydrogen peroxide into the system (as with the previous complex), intense plasmid degradation was observed, forming a smear of DNA under all conditions. This rendered observation of specific bands impossible (columns 8, 9, 10, and 11).

Similar to the two preceding complexes, *fac*-[Re(CO)$_3$(dppz)(py)]$^+$ induced structural alterations in the plasmids (Fig. 8C). The untreated plasmid DNA (lane 2 in the gel) predominantly exhibited a supercoiled intact form (Form I, 62.6%), circular form with single-strand breaks (Form II, 30.9%), and a small percentage in the linear form resulting from double-strand breaks (Form III). Upon treatment with *fac*-[Re(CO)$_3$(dppz)(py)]$^+$, the band profile of the gel was altered, indicating the induction of single-strand breaks (lanes 3, 4, 5, and 6).

In samples treated under non-oxidizing conditions, there was an increase in the percentage of single-stranded breaks (Form II), a significant decrease in the percentage of the intact supercoiled form (Form I), and a slight increase in band density corresponding to double-stranded breaks

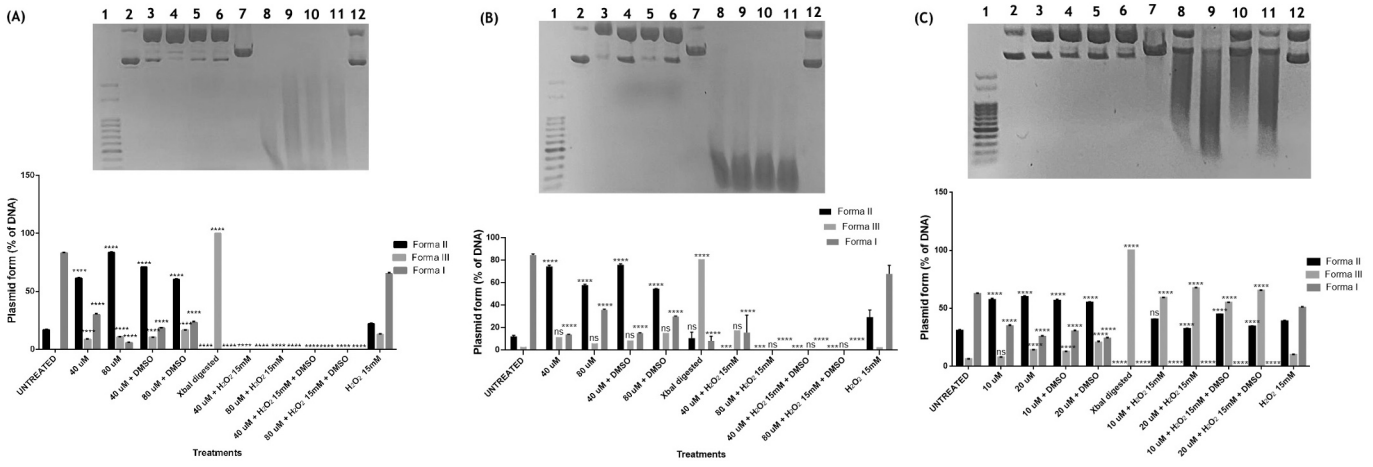

Fig. 8. Agarose gel electrophoresis images of plasmid degradation and band patterns found after treatment with rhenium complexes. **(A)** *fac*-[Re(CO)$_3$(phen)(py)]$^+$, **(B)** *fac*-[Re(CO)$_3$(dpq)(py)]$^+$, and **(C)** *fac*-[Re(CO)$_3$(dppz)(py)]$^+$. 1: Marker; 2: Control without treatment; 3: Re complexes (40 or 10 μM); 4: Re complexes (80 or 20 μM); 5: Re complexes (40 or 10 μM) + DMSO; 6: Re complexes (80 or 20 μM) + DMSO (0.05%); 7: *Xba* I digested; 8: Re complexes (40 or 10 μM) + H_2O_2 (15 mM); 9: Re complexes (80 or 20 μM) + H_2O_2 (15 mM); 10: Re complexes (40 or 10 μM) + H_2O_2 (15 mM) + DMSO (0.05%); 11: Re complexes (80 or 20 μM) + H_2O_2 (15 mM) + DMSO (0.05%); 12: H_2O_2 (15 mM). Data are expressed as the mean ± SE of three assays. Statistical analysis by two-way ANOVA and multiple comparisons by Bonferroni test *$p < 0.05$, **$p < 0.01$, ***$p < 0.001$, ****$p < 0.0001$, ns = not significant compared to the untreated control.

(Form III). The ability for these complexes to cleave plasmid DNA without oxidants or not hydrolytically is unusual and highly unexpected, as rhenium compounds are inert and are unlikely to act as Lewis acid catalysts for this type of cleavage.

The molecular docking data of this work show that rhenium complexes interact with DNA base. The study performed by Knopf et al. (2017) [6] reveals that rhenium complexes can bind covalently to guanine DNA or RNA nucleobase. The exact mechanism of interaction with DNA has not been fully elucidated; however, the study performed by Konovalov et al. in 2020 [60] suggests that ligands composed of benzene rings serve as a driving force for the interaction of rhenium complexes with DNA nucleotide bases by inducing a large number of hydrophobic interactions, rich in π bonding, including π-π stacking, which enhances DNA intercalation. This is corroborated by the presented result of molecular docking, which shows that the more benzene rings present, the higher the affinity to the DNA molecule, as demonstrated by the studied complexes. Another study conducted by Varna et al. in 2020 [57] demonstrates that Rhenium I complexes also have the ability to interact and cleave *S. pombe* genomic DNA, depending on the nature of their ligands. This interaction mechanism requires further studies, as rhenium compounds are inert and do not exhibit this type of catalytic activity in non-oxidizing conditions.

Similar to the two previous complexes, under pro-oxidizing conditions, represented by the introduction of hydrogen peroxide into the system, intense plasmid degradation was observed, forming a DNA smear under all conditions (lanes 8, 9, 10, and 11 in the gel). When we observed the band pattern induced by *fac*-$[Re(CO)_3(dppz)(py)]^+$ treatment under this pro-oxidizing condition, notwithstanding the pronounced degradation of DNA, discernible intact bands persisted, which could be attributed to the lower concentration employed during plasmid treatment. These concentrations were intricately tied to the IC_{50} values specified for each metal complex, with *fac*-$[Re(CO)_3(dppz)(py)]^+$ showing a notably lower IC_{50} concentration than the other complexes.

A consistent pattern was observed in all gel electrophoresis experiments. Column 7 consistently served as a positive control for double-strand breaks, indicating that the plasmid DNA underwent treatment with the single-site restriction enzyme *Xba*I. Column 1 consistently represented the molecular weight markers, providing a reference for the sizing of DNA fragments. Finally, column 12 consistently represented the plasmid that remained untreated with the complex but was exposed to pro-oxidizing conditions. This uniformity in the experimental setup and control columns across all gels ensured a standardized comparison of the results and facilitated an accurate interpretation of the observed outcomes in our study.

All rhenium complexes evaluated in this study exhibited the capacity to induce the cleavage of plasmid DNA in oxidative conditions, thereby substantiating the observations made by previous researchers. Utilizing agarose gel electrophoresis analyses, Varma et al. demonstrated the ability of heteronuclear rhenium(I) complexes to induce DNA cleavage in *Saccharomyces cerevisiae* [58].

Zeleniuk et al. exhibited nucleolytic activity in pUC18 plasmids treated with dirhenium(III) complexes [61]. Similar to the complexes assessed in this study, increased activity was observed in the presence of hydrogen peroxide, concluding that DNA is a potential target in living cells. The authors indicated that the mechanism underlying DNA cleavage in dirhenium(III) complexes is multifaceted, emphasizing the importance of considering the effects of electron donation or withdrawal from ligands, as well as the influence of the catalytic activity of the metal core. These results align with our findings showing that the effect of the rhenium complexes varied, likely because of the different ligands present in each complex.

Ghosh et al. assessed the effects of rhenium(II) dinitrosyl and mononitrosyl complexes on the SC plasmid (pUC19) [59]. Similar to the findings of this study, they observed effective nucleolytic activity in the presence of H_2O_2, cleaving DNA into a circular form with single-strand breaks. According to the authors, the presence of H_2O_2 as an oxidizing agent favors Fenton-type reactions, where oxidation of the metal complex occurs, leading to the formation of more accessible and reactive oxygen species such as hydroxyl radicals ($OH^•$), which attack DNA molecules. The same mechanism is probably responsible for the breaks induced by *fac*-$[Re(CO)_3(phen)(py)]^+$, *fac*-$[Re(CO)_3(dpq)(py)]^+$, and *fac*-$[Re(CO)_3(dppz)(py)]^+$. In the presence of DMSO, the intensity of bands resulting from breaks decreased in some treatments, supporting this hypothesis. This agent acts as a free radical scavenger by neutralizing the reactive species generated.

The present study sheds light on the complex interaction mechanisms between rhenium complexes and DNA, revealing intriguing insights into their potential biological applications. Future studies should focus on elucidating the precise mechanisms of interaction, exploring the effects of different ligands on DNA binding affinity, and investigating the potential therapeutic applications of Rhenium complexes in various disease contexts. By continuing to deepen our understanding of these interactions, we can unlock new opportunities for the development of novel treatments and therapies. Ultimately, collaborative efforts across multidisciplinary research teams will be instrumental in advancing our knowledge and harnessing the full potential of rhenium complexes in biomedicine.

3.11. Cytotoxicity of rhenium(I) tricarbonyl complexes

Given the reported anticancer activity of rhenium(I) tricarbonyl complexes [1,2,62] and considering that the inherent cytotoxicity of the complexes is contingent on the chemical nature of the molecules ligands [63], we evaluated the *in vitro* cytotoxicity of *fac*-$[Re(CO)_3(phen)(py)]^+$, *fac*-$[Re(CO)_3(dpq)(py)]^+$, and *fac*- $[Re(CO)_3(dppz)(py)]^+$ in HeLa, PNT2, B16F10, and NIH-3 T3 cells by the MTT assay. The half-maximal inhibitory concentration (IC_{50}) of each compound was determined (Table 8) from a dose-response curve of cell viability *versus* log(concentration) (Fig. S10 in the supplemental material).

IC_{50} data indicates that the cytotoxic activity of the examined Re(I) complexes increased with the expansion of the π-system of the ligands in all cell lines: $IC_{50}^{Re(dppz)} < IC_{50}^{Re(dpq)} < IC_{50}^{Re(phen)}$ (Table 8). This explains how the chemical structure of the ligands influenced the overall cytotoxicity of the studied rhenium complexes, as shown in other studies [4,11,63,64].

The *fac*-$[Re(CO)_3(phen)(py)]^+$ complex showed an IC_{50} of 32.57 μM against HeLa cells. However, its IC_{50} exceeded the highest tested dose of 100 μM for all the other cell lines tested, rendering it impractical to calculate its SI. The *fac*-$[Re(CO)_3(dpq)(py)]^+$ complex exhibited an IC_{50} of 26.67 μM for the HeLa strain, with an SI of 1.57, whereas for the B16F10 strain, the IC_{50} was 43.61 μM with an SI of 1.44 (Table 8). The *fac*-$[Re(CO)_3(dppz)(py)]^+$ complex showed an IC_{50} of 8.48 μM for HeLa with a SI of 1.91, whereas for the B16F10 strain, the IC_{50} was 11.51 μM, and the SI was 1.62 (Table 8).

Table 8
IC_{50} of rhenium complexes in different cell lines and their respective selectivity indices (SI). Values correspond to the average ± standard error of two separate assays ($n = 6$).

Rhenium(I) complex	IC_{50} (μM)		SI	IC_{50} (μM)		SI
	HeLa	PNT2		B16F10	NIH/3 T3	
fac-[Re $(CO)_3$(phen) (py)]$^+$	32.57 ± 0.06	>100	ND*	>100	>100	ND*
fac- [Re $(CO)_3$(dpq) (py)]$^+$	26.67 ± 0.05	41.77 ± 4.5	1.57	43.61 ± 3.26	62.66 ± 2.3	1.44
fac- [Re $(CO)_3$(dppz) (py)]$^+$	8.48 ± 0.03	16.23 ± 0.97	1.91	11.51 ± 0.61	18.63 ± 0.86	1.62

* ND = Not Defined.

The *fac*-$[Re(CO)_3(dppz)(py)]^+$ complex showed significantly higher cytotoxicity toward all cell lines than the other two Re(I) complexes (Table 8). Lower IC_{50} value of *fac*-$[Re(CO)_3(dppz)(py)]^+$ (IC_{50} = 8.48 μM, Table 8) with respect to the HeLa cell line was comparable to that of a similar compound reported in literature, which also comprised the dppz ligand: *fac*-$[Re(CO)_3(dppz)(nHO)]^+$ (IC_{50} = 10 μM) [63]. Notably, the IC_{50} value of cisplatin was approximately 25 μM against the same cell line [4,65].

Pete *et al* [66] reported the IC_{50} values of rhenium complexes against HeLa described by various authors, which ranged from 36 to 371 μM. These data corroborate the range of IC_{50} values found in the present study, where the three analyzed Re complexes showed lower IC_{50} values than those described for the other complexes, demonstrating greater cytotoxicity compared to the complexes described in the literature [66].

The SI is crucial for understanding the selectivity of compounds toward tumor cells *versus* normal cells [67]. The SI values obtained for all rhenium complexes were < 2, (the SI for HeLa cells was 1.91), indicating that targeted delivery or bioisosterism strategies should be used to improve the selectivity of the complex. According to the classification described by Bauer et al., the Re complexes examined in this study can be considered moderately toxic to the HeLa strain, since all IC_{50} values were lower than 50 μM [68].

A control assay was performed to evaluate the toxicity of the isolated ligand and compare it with its corresponding complex. Results indicated that the cytotoxicity of the *fac*-$[Re(CO)_3(dppz)(py)]^+$ complex was significantly greater than that of its dppz ligand (Fig. S11 in the supplemental material), confirming the cytotoxicity of the *fac*-$[Re(CO)_3(dppz)(py)]^+$ complex, rather than solely the dppz ligand. Therefore, *fac*-$[Re(CO)_3(dppz)(py)]^+$ may represent a promising an antitumor drug candidate.

3.12. Anti-proliferative activity in HeLa: effects on the cell cycle

To assess the impact of *fac*-$[Re(CO)_3(phen)(py)]^+$, *fac*-$[Re(CO)_3(dpq)(py)]^+$, and *fac*-$[Re(CO)_3(dppz)(py)]^+$) on cell proliferation, the HeLa cell line was treated with the complexes for 24 h, and the distribution of cells in each phase of the cell cycle was evaluated by flow cytometry after staining the cell nuclei with propidium iodide. An increase in the number of cells in the G0/G1 and/or G2 phases was observed after 24 h of treatment with all the studied rhenium complexes.

Regarding the *fac*-$[Re(CO)_3(phen)(py)]^+$ complex, at a treatment concentration of 20 μM, approximately 57.9% of cells were in the G0/G1 phase (Fig. 9A). This result was in contrast with the control group, which recorded a proportion of 49.4%. Additionally, in groups treated with concentrations of 10 μM and 40 μM, the percentages were approximately 55.2% and 59.5%, respectively. Simultaneously, the compound reduced the number of cells in the S phase of the cell cycle while demonstrating a proportional increase in the number of cells in the G2 phase. This phenomenon manifested in a dose-dependent manner, highlighting the role of cell cycle regulation. The complex demonstrated a remarkable inhibitory effect on cell proliferation by trapping cells in the G0/G1 and G2 phases (Fig. 8A).

Concerning the complex *fac*-$[Re(CO)_3(dpq)(py)]^+$, a significant increase in the percentage of cells in the G0/G1 phase was observed, increasing from 49.4% in the control group to approximately 74.8% in the group subjected to treatment with 20 μM (Fig. 9B). Additionally, under experimental conditions with concentrations of 10 μM and 40 μM, values of approximately 60.3% and 59.7% were recorded, respectively. Notably, the compound consistently reduced the number of cells in the S phase of the cell cycle, coupled with a gradual increase in the proportion of cells in the G2 phase recorded with an increase in the concentration. As previously observed, this phenomenon followed a dose-dependent relationship, reinforcing the hypothesis of cell cycle modulation by this complex. Similar to the previously reported complex, *fac*-$[Re(CO)_3(dpq)(py)]^+$ inhibited cell proliferation. This inhibition was manifested by the trapping of cells in the G0/G1 and G2 phases, as shown in Fig. 9B.

In the analyses of the *fac*-$[Re(CO)_3(dppz)(py)]^+$ complex, an increase in the number of cells in the G0/G1 phase was observed from 49.4% in the control group to 57.5% in cells subjected to treatment with a concentration of 10 μM (Fig. 9C). Additionally, under experimental conditions where concentrations were fixed at 5 μM and 20 μM, the percentages were calculated at 53.5% and 46.3%, respectively. Furthermore, it is notable that the compound exhibited a consistent trend of reduction in cells in the S phase of the cell cycle, coupled with a gradual increase in the proportion of cells in the G2 phase with the increase in the concentration of the complex; approximately 40% of cells were found in the G2 phase upon treatment with 20 μM. This dose-dependent relationship highlights the direct influence of the compound on the cell cycle stages. Consistent with the results observed for previous compounds, *fac*-$[Re(CO)_3(dppz)(py)]^+$ also stands out for its ability to inhibit cell proliferation. This inhibitory effect was supported by the observation of cell trapping in the G0/G1 and G2 phases, as depicted in Fig. 9C.

In the context of the intrinsic cellular division process, checkpoint verification mechanisms, when activated in response to DNA damage, impede half of the progression of the cell cycle. This translates into the trapping of cells in specific phases, such as G0/G1, as demonstrated by Machado et al. in 2021 with a copper complex, or even in the G2 phase [69], as evidenced by Simpson et al. in 2017 while studying tricarbonyl rhenium complexes [70]. These observations are consistent with the results of the present study. When the cell cycle is blocked during these phases, two possible pathways emerge. The first pathway involves the repair of cellular damage, whereas the second can trigger the process of programmed cell death, known as apoptosis, a phenomenon observed in cells treated with the three complexes used in this study.

4. Conclusions

In vitro and *in silico* interaction studies of rhenium complexes with biomolecules (proteins, DNA, and lipids) revealed that greater hydrophobicity of the ligands in the complexes can favor interactions with biomolecules and consequently increase cytotoxicity in cells. The Re(I) complex containing the dppz ligand exhibited the highest cytotoxicity among the studied compounds, probably because of its lipophilicity and stronger biomolecular interactions. These interactions induced cell-cycle arrest, culminating in programmed cell death. Our findings emphasize the importance of considering these characteristics in rational drug design.

Funding

This work was supported by Fundação de Amparo à Pesquisa de Minas Gerais/FAPEMIG (APQ-00704-21 and APQ-01087-21) and Conselho Nacional de Desenvolvimento Científico e Tecnológico/CNPq (407282/2023–8). Tayana M. Tsubone expresses gratitude to the L'Oréal Brazil-UNESCO-ABC Award "*For Women in Science*" 2023, in chemistry field. This study was financed in part by the Coordenação de Aperfeiçoamento de Pessoal de Nível Superior/CAPES - Finance Code 001 and CAPES scholarship grant 88887.828352/2023–00.

CRediT authorship contribution statement

Tayná Saraiva de Lavor: Methodology, Investigation, Formal analysis. **Maria Henriqueta Silvestre Teixeira:** Methodology, Investigation, Formal analysis. **Patrícia Alves de Matos:** Investigation, Formal analysis. **Ricardo Campos Lino:** Investigation, Formal analysis. **Clara Maria Faria Silva:** Investigation, Formal analysis. **Marcos Eduardo Gomes do Carmo:** Investigation, Formal analysis. **Marcelo Emílio Beletti:** Resources. **Antonio Otavio T. Patrocinio:** Validation, Resources, Formal analysis. **Robson José de Oliveira Júnior:** Writing – review & editing, Writing – original draft, Validation, Supervision,

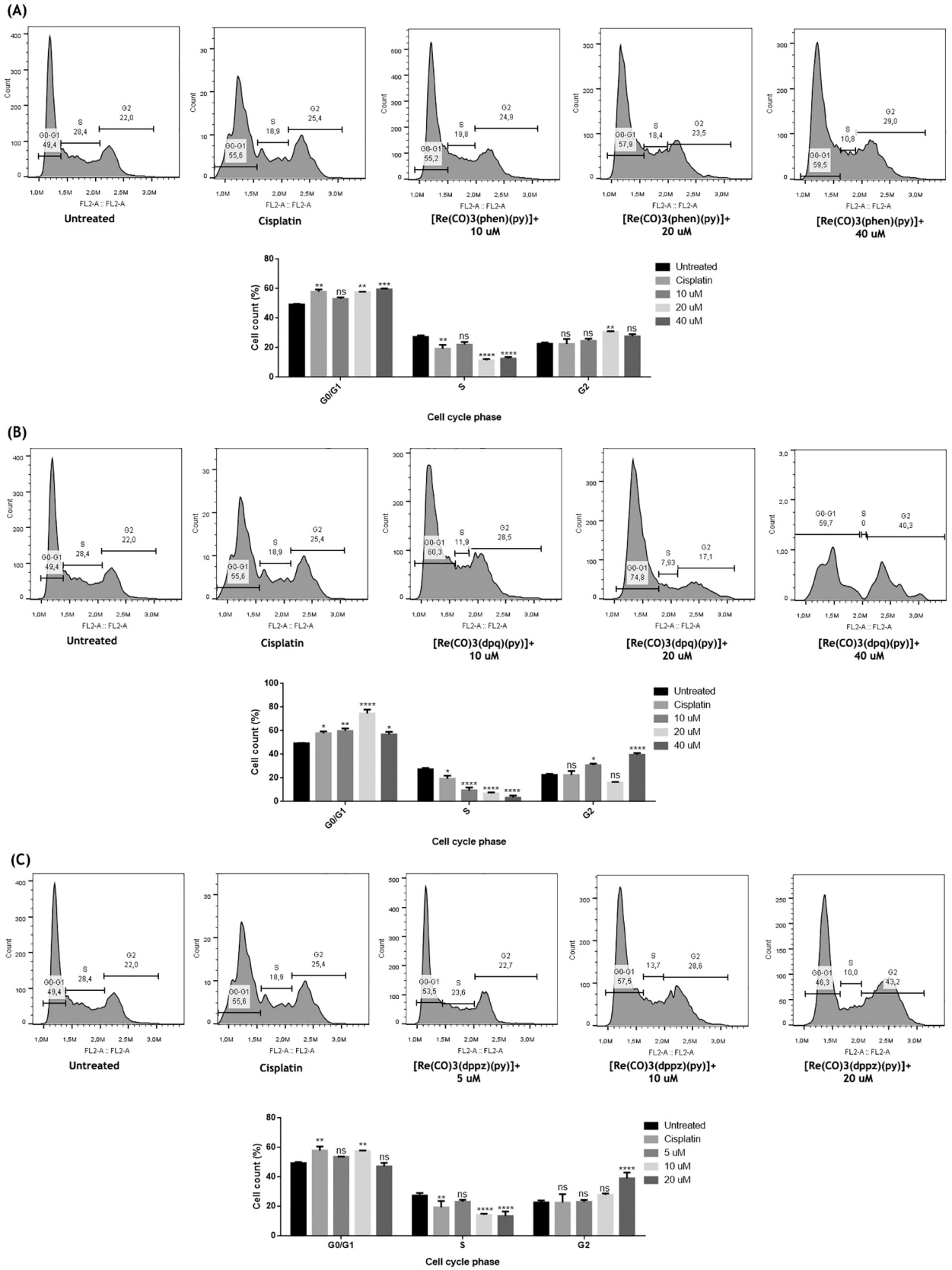

Fig. 9. Representative histograms of the cell cycle phases of HeLa tumorigenic cells treated with different concentrations of rhenium complexes. **(A)** *fac*-[Re(CO)$_3$(phen)(py)]$^+$, **(B)** *fac*-[Re(CO)$_3$(dpq)(py)]$^+$ and **(C)** *fac*-[Re(CO)$_3$(dppz)(py)]$^+$. For the bar graph, the data represent the mean ± standard error. *$p < 0.05$. **$p < 0.01$, ***$p < 0.001$, and ****$p < 0.0001$ (compared to the negative control by one-way ANOVA followed by Bonferroni post-test).

Resources, Formal analysis. **Tayana Mazin Tsubone:** Writing – review & editing, Writing – original draft, Visualization, Validation, Supervision, Resources, Project administration, Methodology, Funding acquisition, Formal analysis, Conceptualization.

Declaration of competing interest

The authors declare that they have no known competing financial interests or personal relationships that could have appeared to influence the work reported in this paper.

Data availability

Data will be made available on request.

Acknowledgments

The authors acknowledge the National Institute of Science and Technology in Theranostics and Nanobiotechnology, INCT–Teranano, and the Laboratory of Biotechnology, Professor Dr. Luiz Ricardo Goulart. We thank Professor Renata Galvão de Lima (ICENP – UFU) for support with the DNA assays.

Appendix A. Supplementary data

Supplementary data to this article can be found online at https://doi.org/10.1016/j.jinorgbio.2024.112600.

References

[1] A. Leonidova, G. Gasser, Underestimated potential of organometallic rhenium complexes as anticancer agents, ACS Chem. Biol. 9 (2014) 2180–2193, https://doi.org/10.1021/cb500528c.
[2] A. Sharma, B. Kar, U. Das, P. Paira, Target-specific mononuclear and binuclear rhenium(i) tricarbonyl complexes as upcoming anticancer drugs, RSC Adv. 12 (2022) 20264–20295, https://doi.org/10.1039/D2RA03434D.
[3] S. Hostachy, C. Policar, N. Delsuc, Re(I) carbonyl complexes: multimodal platforms for inorganic chemical biology, Coord. Chem. Rev. 351 (2017) 172–188, https://doi.org/10.1016/j.ccr.2017.05.004.
[4] P.-X. Yang, K. Xie, M.-R. Chen, Z. Zhang, B. Huang, R.-T. Li, R.-R. Ye, Synthesis, characterization, and antitumor mechanism investigation of ruthenium(II)/rhenium(I)-daminozide conjugates, Inorganics 11 (2023) 142, https://doi.org/10.3390/inorganics11040142.
[5] W. Wang, Y. Kai, T.S.A. Hor, J.J. Vittal, J.R. Wheaton, I.H. Hall, Synthesis, X-ray structures, and cytotoxicity of rhenium (I) carbonyl 2- (dimethylamino) ethoxide complexes, Polyhedron 21 (2002) 1991–1999.
[6] K.M. Knopf, B.L. Murphy, S.N. Macmillan, J.M. Baskin, M.P. Barr, E. Boros, J. J. Wilson, In vitro anticancer activity and in vivo biodistribution of rhenium(I) tricarbonyl aqua complexes, J. Am. Chem. Soc. 139 (2017) 14302–14314, https://doi.org/10.1021/jacs.7b08640.
[7] C.C. Konkankit, A.P. King, K.M. Knopf, T.L. Southard, J.J. Wilson, In vivo anticancer activity of a rhenium(I) tricarbonyl complex, ACS Med. Chem. Lett. 10 (2019) 822–827, https://doi.org/10.1021/acsmedchemlett.9b00128.
[8] D.-L. Ma, C.-M. Che, F.-M. Siu, M. Yang, K.-Y. Wong, DNA binding and cytotoxicity of ruthenium(II) and rhenium(I) complexes of 2-amino-4-phenylamino-6-(2-pyridyl)-1,3,5-triazine, Inorg. Chem. 46 (2007) 740–749, https://doi.org/10.1021/ic061518s.
[9] J. Zhang, J.J. Vittal, W. Henderson, J.R. Wheaton, I.H. Hall, T.S.A. Hor, Y. Kai, Tricarbonylrhenium(I) complexes of phosphine-derivatized amines, amino acids and a model peptide: structures, solution behavior and cytotoxicity, J. Organomet. Chem. 650 (2002) 123–132, https://doi.org/10.1016/S0022-328X(02)01200-7.
[10] L.E. Enslin, K. Purkait, M.D. Pozza, B. Saubamea, P. Mesdom, H.G. Visser, G. Gasser, M. Schutte-Smith, Rhenium(I) tricarbonyl complexes of 1,10-phenanthroline derivatives with unexpectedly high cytotoxicity, Inorg. Chem. 62 (2023) 12237–12251, https://doi.org/10.1021/acs.inorgchem.3c00730.
[11] C.C. Konkankit, B.A. Vaughn, Z. Huang, E. Boros, J.J. Wilson, Systematically altering the lipophilicity of rhenium(i) tricarbonyl anticancer agents to tune the rate at which they induce cell death, Dalton Trans. 49 (2020) 16062–16066, https://doi.org/10.1039/D0DT01097A.
[12] J.E. Dickeson, L.A. Summers, Derivatives of 1,10-phenanthroline-5,6-quinone, Aust. J. Chem. 23 (1970) 1023–1027.
[13] M. Yamada, Y. Tanaka, Y. Yoshimoto, S. Kuroda, I. Shimao, Synthesis and properties of diamino-substituted dipyrido [3,2- a : 2′,3′- c]phenazine, Bull. Chem. Soc. Jpn. 65 (1992) 1006–1011, https://doi.org/10.1246/bcsj.65.1006.
[14] M. Arias, J. Concepción, I. Crivelli, A. Delgadillo, R. Díaz, A. Francois, F. Gajardo, R. López, A.M. Leiva, B. Loeb, Influence of ligand structure and molecular geometry on the properties of d6 polypyridinic transition metal complexes, Chem. Phys. 326 (2006) 54–70, https://doi.org/10.1016/j.chemphys.2006.01.040.
[15] C.L. Ramos, F.S. Prado, M.E.G. Carmo, G. Farias, B. Souza, A.E.H. MacHado, A.O. T. Patrocinio, Temperature dependent emission properties of ReI tricarbonyl complexes with dipyrido-quinoxaline and phenazine ligands, J. Braz. Chem. Soc. 33 (2022) 425–436, https://doi.org/10.21577/0103-5053.20210161.
[16] S.F. Sousa, R.N. Sampaio, N.M. Barbosa Neto, A.E.H. Machado, A.O.T. Patrocinio, The photophysics of fac-[re(CO)3(NN)(bpa)]+ complexes: a theoretical/experimental study, Photochem. Photobiol. Sci. 13 (2014) 1213–1224, https://doi.org/10.1039/c4pp00074a.
[17] F.S. Prado, S.F. Sousa, A.E.H. Machado, A.O.T. Patrocinio, Influence of the protonatable site in the photo-induced proton-coupled electron transfer between rhenium (I) Polypyridyl complexes and hydroquinone, J. Braz. Chem. Soc. 28 (2017) 1741–1751, https://doi.org/10.21577/0103-5053.20170022.
[18] L.A. Faustino, A.E. Hora Machado, A.O.T. Patrocinio, Photochemistry of fac-[Re(CO)3(dcbH2)(trans-stpy)]+: new insights on the isomerization mechanism of coordinated stilbene-like ligands, Inorg. Chem. 57 (2018) 2933–2941, https://doi.org/10.1021/acs.inorgchem.8b00093.
[19] A.O.T. Patrocinio, M.K. Brennaman, T.J. Meyer, N.Y. Murakami Iha, Excited-state dynamics in fac-[re(CO)3(Me4phen)(L)]+, J. Phys. Chem. A 114 (2010) 12129–12137, https://doi.org/10.1021/jp104692w.
[20] B.M. Rodrigues, H.F.V. Victória, G. Leite, K. Krambrock, O.A. Chaves, D.F. de Oliveira, R.Q. de Garcia, L. De Boni, L.A.S. Costa, B.A. Iglesias, Photophysical, photobiological, and biomolecule-binding properties of new tri-cationic meso-tri (2-thienyl)corroles with Pt(II) and Pd(II) polypyridyl derivatives, J. Inorg. Biochem. 242 (2023) 112149, https://doi.org/10.1016/j.jinorgbio.2023.112149.
[21] A.P. Gerola, T.M. Tsubone, A. Santana, H.P.M. De Oliveira, N. Hioka, W. Caetano, Properties of chlorophyll and derivatives in homogeneous and microheterogeneous systems, J. Phys. Chem. B 115 (2011) 7364–7373, https://doi.org/10.1021/jp201278b.
[22] J.C. Dearden, Partitioning and lipophilicity in quantitative structure-activity relationships, Environ. Health Perspect. 61 (1985) 203–228, https://doi.org/10.1289/ehp.8561203.
[23] J.R. Lakowicz, Principles of Fluorescence Spectroscopy, 1983, https://doi.org/10.1007/978-0-387-46312-4.
[24] J.R. Lakowicz, Principles of Fluorescence Spectroscopy, 2006.
[25] C. Has, P. Sunthar, A comprehensive review on recent preparation techniques of liposomes, J. Liposome Res. 30 (2020) 336–365, https://doi.org/10.1080/08982104.2019.1668010.
[26] A.D. Bangham, R.W. Horne, Negative staining of phospholipids and their structural modification by surface-active agents as observed in the electron microscope, J. Mol. Biol. 8 (1964) 660–668, https://doi.org/10.1016/S0022-2836(64)80115-7.
[27] H. Zhang, Thin-film hydration followed by extrusion method for liposome preparation, in: liposomes, Methods Mol. Biol. 1522 (2017) 17–22, https://doi.org/10.1007/978-1-4939-6591-5_2.
[28] A. Karewicz, D. Bielska, B. Gzyl-Malcher, M. Kepczynski, R. Lach, M. Nowakowska, Interaction of curcumin with lipid monolayers and liposomal bilayers, Colloids Surf. B: Biointerfaces 88 (2011) 231–239, https://doi.org/10.1016/j.colsurfb.2011.06.037.
[29] N.C. Santos, M. Prieto, M.A.R.B. Castanho, Quantifying molecular partition into model systems of biomembranes : an emphasis on optical spectroscopic methods 1612 (2003) 123–135, https://doi.org/10.1016/S0005-2736(03)00112-3.
[30] M. Sirajuddin, S. Ali, A. Badshah, Drug–DNA interactions and their study by UV–visible, fluorescence spectroscopies and cyclic voltametry, J. Photochem. Photobiol. B Biol. 124 (2013) 1–19, https://doi.org/10.1016/j.jphotobiol.2013.03.013.
[31] C.F.N. da Silva, P.B.H. Chrispim, B. Possato, G.B. Portapilla, T.N. Rohrabaugh, L.C. B. Ramos, R. Santana da Silva, S. de Albuquerque, C. Turro, S. Nikolaou, Anticancer and antitrypanosomal activities of trinuclear ruthenium compounds with orthometalated phenazine ligands, Dalton Trans. 49 (2020) 16440–16452, https://doi.org/10.1039/D0DT01035A.
[32] V. Gonzlez-Ruiz, A.I.M. Antonia, P. Ribelles, M. Teresa, J. Carlos, An overview of analytical techniques employed to evidence drug-DNA interactions. Applications to the design of genosensors, in: Biomed. Eng. Trends, Res. Technol., InTech, 2011, https://doi.org/10.5772/13586.
[33] M.E. Reichmann, S.A. Rice, C.A. Thomas, P. Doty, A further examination of the molecular weight and size of desoxypentose nucleic acid, J. Am. Chem. Soc. 76 (1954) 3047–3053, https://doi.org/10.1021/ja01640a067.
[34] H.A. Benesi, J.H. Hildebrand, A spectrophotometric investigation of the interaction of iodine with aromatic hydrocarbons, J. Am. Chem. Soc. 71 (1949) 2703–2707, https://doi.org/10.1021/ja01176a030.
[35] G.F. Shen, T.T. Liu, Q. Wang, M. Jiang, J.H. Shi, Spectroscopic and molecular docking studies of binding interaction of gefitinib, lapatinib and sunitinib with bovine serum albumin (BSA), J. Photochem. Photobiol. B Biol. 153 (2015) 380–390, https://doi.org/10.1016/j.jphotobiol.2015.10.023.
[36] F. Kheirdoosh, M. Pazhavand, M. Sariaslani, N.H. Moghadam, S. Salehzadeh, Multi-spectroscopic and molecular docking studies on the interaction of neotame with calf thymus DNA, Nucleosides Nucleotides Nucleic Acids 39 (2020) 699–714, https://doi.org/10.1080/15257770.2019.1680999.
[37] T. Mosmann, Rapid colorimetric assay for cellular growth and survival: application to proliferation and cytotoxicity assays, J. Immunol. Methods 65 (1983) 55–63, https://doi.org/10.1016/0022-1759(83)90303-4.
[38] T.L. Riss, R.A. Moravec, A.L. Niles, S. Duellman, H.A. Benink, T.J. Worzella, L. Minor, Cell Viability Assays, 2004.
[39] D.A. Paixão, B.C.A. de Oliveira, J.C. Almeida, L.M. Sousa, C.D. Lopes, Z. A. Carneiro, D.Y. Tezuka, J.C.T. Clavijo, J. Ellena, L. Polloni, P.H.A. Machado, S. de

Albuquerque, R.J. de Oliveira Júnior, S. Guilardi, W. Guerra, Crystal structure, anti-Trypanosoma cruzi and cytotoxic activities of cu(II) complexes bearing β-diketone and α-diimine ligands, Inorg. Chim. Acta 499 (2020) 119164, https://doi.org/10.1016/j.ica.2019.119164.
[40] A.K. Ghose, V.N. Viswanadhan, J.J. Wendoloski, A knowledge-based approach in designing combinatorial or medicinal chemistry libraries for drug discovery. 1. A qualitative and quantitative characterization of known drug databases, J. Comb. Chem. 1 (1999) 55–68, https://doi.org/10.1021/cc9800071.
[41] C.-M. Hsieh, S. Wang, S.-T. Lin, S.I. Sandler, A predictive model for the solubility and octanol−water partition coefficient of pharmaceuticals, J. Chem. Eng. Data 56 (2011) 936–945, https://doi.org/10.1021/je1008872.
[42] B. Hamelin, Hydrophilicity/ lipophilicity: relevance for the pharmacology and clinical effects of HMG-CoA reductase inhibitors, Trends Pharmacol. Sci. 19 (1998) 26–37, https://doi.org/10.1016/S0165-6147(97)01147-4.
[43] F. Ragone, H.H.M. Saavedra, P.F. García, E. Wolcan, G.A. Argüello, G.T. Ruiz, Association studies to transporting proteins of fac-ReI(CO)3(pterin)(H2O) complex, JBIC J. Biol. Inorg. Chem. 22 (2017) 99–108, https://doi.org/10.1007/s00775-016-1410-7.
[44] G. Balakrishnan, T. Rajendran, K.S. Murugan, M. Ganesan, V.K. Sivasubramanian, S. Rajagopal, Synthesis, photophysics and the binding studies of rhenium(I) diimine surfactant complexes with serum albumins: a spectroscopic and docking study approach, JOL 205 (2019) 51–60, https://doi.org/10.1016/j.jlumin.2018.08.078.
[45] K.P.M. Frin, V.M. Nascimento, Rhenium(I) polypyridine complexes as luminescence-based sensors for the BSA protein, J. Braz. Chem. Soc. (2015), https://doi.org/10.5935/0103-5053.20150268.
[46] M.P. Coogan, V. Fernández-Moreira, J.B. Hess, S.J.A. Pope, C. Williams, Rhenium fac-tricarbonyl bisimine complexes: luminescence modulation by hydrophobically driven intramolecular interactions, New J. Chem. 33 (2009) 1094, https://doi.org/10.1039/b819453j.
[47] B.J. Pages, D.L. Ang, E.P. Wright, J.R. Aldrich-Wright, Metal complex interactions with DNA, Dalton Trans. 44 (2015) 3505–3526, https://doi.org/10.1039/C4DT02700K.
[48] S.U. Rehman, T. Sarwar, M.A. Husain, H.M. Ishqi, M. Tabish, Studying non-covalent drug–DNA interactions, Arch. Biochem. Biophys. 576 (2015) 49–60, https://doi.org/10.1016/j.abb.2015.03.024.
[49] S.R. Dalton, Æ.S. Glazier, S.J.N. Burgmayer, DNA binding by Ru(II)– bis (bipyridine)– pteridinyl complexes, J. Biol. Inorg. Chem. 13 (2008) 1133–1148, https://doi.org/10.1007/s00775-008-0399-y.
[50] A. Ashok, S. Banerjee, N. Anand, A. Banerjee, Spectroscopic and viscometric determination of DNA-binding modes of some bioactive dibenzodioxins and phenazines, Biochem. Biophys. Rep. 18 (2019) 100629, https://doi.org/10.1016/j.bbrep.2019.100629.
[51] E. Tri, D.H. Tjahjono, N. Yoshioka, H. Inoue, Spectrochimica Acta part a : molecular and biomolecular spectroscopy spectroscopic studies on the thermodynamic and thermal denaturation of the ct-DNA binding of methylene blue, Spectrochim, Acta Part A Mol. Biomol. Spectrosc. 77 (2010) 528–534, https://doi.org/10.1016/j.saa.2010.06.032.
[52] N. Shahabadi, F. Shiri, R. Khodarahmi, A cu (I) complex groove binder with a high affinity towards DNA denaturation, J. Mol. Liq. 345 (2022) 117904, https://doi.org/10.1016/j.molliq.2021.117904.
[53] A. Rodger, Circular and linear dichroism of drug-DNA systems, in: Drug-DNA Interact. Protoc., 2009, pp. 37–54, https://doi.org/10.1007/978-1-60327-418-0.
[54] F.L. Thorp-Greenwood, M.P. Coogan, L. Mishra, N. Kumari, G. Rai, S. Saripella, The importance of cellular localisation of probes: synthesis, photophysical properties, DNA interactions and cellular imaging properties of rhenium dppz complexes with known cellular localisation vectors, New J. Chem. 36 (2012) 64–72, https://doi.org/10.1039/C1NJ20662A.
[55] M.B. Ismail, I.N. Booysen, M.P. Akerman, DNA interaction studies of rhenium compounds with schiff base chelates encompassing biologically relevant moieties, Nucleosides Nucleotides Nucleic Acids 38 (2019) 950–971, https://doi.org/10.1080/15257770.2019.1639058.
[56] W.S. Magalhães, C.M. Corrêa, R.B. De Alencastro, T.J. Nagem, Bases moleculares da ação anti-inflamatória dos ácidos oleanólico e ursólico sobre as isoformas da ciclo-oxigenase por docking e dinâmica molecular, Quim Nova 35 (2012) 241–248, https://doi.org/10.1590/S0100-40422012000200003.
[57] R.R. Varma, B.H. Pursuwani, E. Suresh, B.S. Bhatt, M.N. Patel, Single crystal, DNA interaction and cytotoxicity studies of rhenium(I) organometallic compounds, J. Mol. Struct. 1200 (2020) 127068, https://doi.org/10.1016/j.molstruc.2019.127068.
[58] R.R. Varma, J.G. Pandya, F.U. Vaidya, C. Pathak, R.A. Dabhi, M.P. Dhaduk, B. S. Bhatt, M.N. Patel, DNA interaction, anticancer, antibacterial, ROS and lipid peroxidation studies of quinoxaline based organometallic re(I) carbonyls, J. Mol. Struct. 1240 (2021) 130529, https://doi.org/10.1016/j.molstruc.2021.130529.
[59] S. Ghosh, S.S. Paul, J. Mitra, K.K. Mukherjea, Rhenium(II) nitrosyl complexes: synthesis, characterization, DFT calculations and DNA nuclease activity, J. Coord. Chem. 67 (2014) 1809–1834, https://doi.org/10.1080/00958972.2014.924622.
[60] D.I. Konovalov, A.A. Ivanov, T.S. Frolova, I.V. Eltsov, Y.M. Gayfulin, L. Plunkett, M. Bazzar, A.M. Adawi, J.S.G. Bouillard, S.I. Baiborodin, O.I. Sinitsyna, N. V. Kuratieva, V.V. Yanshole, O.A. Efremova, M.A. Shestopalov, Water-soluble rhenium clusters with Triazoles: the effect of chemical structure on cellular internalization and the DNA binding of the complexes, Chem. Eur. J. 26 (2020) 13904–13914, https://doi.org/10.1002/chem.202001680.
[61] K.V. Zeleniuk, O.A. Golichenko, A.V. Shtemenko, N.I. Shtemenko, Further evidence for redox activation of the plasmid – dirhenium(III) complexes interactions, J. V. N. Karazin Kharkiv Natl. Univ. Ser. Biol. (2020) 11–17, https://doi.org/10.26565/2075-5457-2020-34-1.
[62] J. Delasoie, A. Pavic, N. Voutier, S. Vojnovic, A. Crochet, J. Nikodinovic-Runic, F. Zobi, Identification of novel potent and non-toxic anticancer, anti-angiogenic and antimetastatic rhenium complexes against colorectal carcinoma, Eur. J. Med. Chem. 204 (2020) 112583, https://doi.org/10.1016/j.ejmech.2020.112583.
[63] I. Maisuls, E. Wolcan, O.E. Piro, E.E. Castellano, G. Petroselli, R. Erra-Balsells, F. M. Cabrerizo, G.T. Ruiz, Synthesis, structural characterization and biological evaluation of rhenium(I) tricarbonyl complexes with β-carboline ligands, ChemistrySelect 2 (2017) 8666–8672, https://doi.org/10.1002/slct.201701961.
[64] B.L. Murphy, S.C. Marker, V.J. Lambert, J.J. Woods, S.N. MacMillan, J.J. Wilson, Synthesis, characterization, and biological properties of rhenium(I) tricarbonyl complexes bearing nitrogen-donor ligands, J. Organomet. Chem. 907 (2020) 121064, https://doi.org/10.1016/j.jorganchem.2019.121064.
[65] M. Becit, S. Aydın Dilsiz, N. Başaran, Interaction of curcumin on cisplatin cytotoxicity in HeLa and HepG2 carcinoma cells, İstanbul J. Pharm. 50 (2020), https://doi.org/10.26650/IstanbulJPharm.2020.0039.
[66] S. Pete, N. Roy, B. Kar, P. Paira, Construction of homo and heteronuclear Ru(II), Ir (III) and re(I) complexes for target specific cancer therapy, Coord. Chem. Rev. 460 (2022) 214462, https://doi.org/10.1016/j.ccr.2022.214462.
[67] A.A. Pereira, R.H. Piccoli, N.N. Batista, N.G. Camargos, M.M.M. de Oliveira, Thermochemical inactivation of *Escherichia coli, Staphylococcus aureus* and *Salmonella enterica* enteritidis by essencial oils, Cienc. Rural 44 (2014) 2022–2028, https://doi.org/10.1590/0103-8478cr20140092.
[68] E.B. Bauer, A.A. Haase, R.M. Reich, D.C. Crans, F.E. Kühn, Organometallic and coordination rhenium compounds and their potential in cancer therapy, Coord. Chem. Rev. 393 (2019) 79–117, https://doi.org/10.1016/j.ccr.2019.04.014.
[69] P.H.A. Machado, D.A. Paixão, R.C. Lino, T.R. de Souza, N.J. de Souza Bontempo, L. M. Sousa, F. Van Petten de Vasconcelos Azevedo, P.C. Orsolin, P.M.A.P. Lima, I. C. Martins, J.F. da Costa Guerra, S.C. Teixeira, T.G. Araújo, L.R. Goulart, S. Morelli, W. Guerra, R.J. de Oliveira, A selective CuII complex with 4-fluorophenoxyacetic acid hydrazide and phenanthroline displays DNA-cleaving and pro-apoptotic properties in cancer cells, Sci. Rep. 11 (2021) 1–15, https://doi.org/10.1038/s41598-021-03909-1.
[70] P.V. Simpson, I. Casari, S. Paternoster, B.W. Skelton, M. Falasca, M. Massi, Defining the anti-cancer activity of tricarbonyl rhenium complexes: induction of G2/M cell cycle arrest and blockade of aurora-a kinase phosphorylation, Chem. A Eur. J. 23 (2017) 6518–6521, https://doi.org/10.1002/chem.201701208.